Received January 30, 2020, accepted February 17, 2020, date of publication February 27, 2020, date of current version March 11, 2020.

Digital Object Identifier 10.1109/ACCESS.2020.2976772

Detection System for Capacitive Plantar Pressure Monitoring

TZUNG-MIN TSAI, (Student Member, IEEE), SHUENN-YUH LEE, (Senior Member, IEEE), AND SOON-JYH CHANG, (Member, IEEE)

Department of Electrical Engineering, National Cheng Kung University, Tainan City 70101, Taiwan

Corresponding author: Shuenn-Yuh Lee (ieesyl@mail.ncku.edu.tw)

This work was supported in part by the Taiwan Semiconductor Research Institute and the Ministry of Science and Technology (MOST), Taiwan, under Grant MOST 108-2218-E-006-020, Grant MOST 108-2622-8-006-004-TE2, and Grant MOST 109-2622-8-006-021-TE2.

ABSTRACT This study presents a detection system with a prototype acquisition module and display interface for capacitive plantar pressure monitoring. The detection system mainly focuses on a system-level design (not a system on chip). The prototype acquisition module consists of commercial ICs and self-designed chips: A capacitance-to-voltage converter (CVC) and a 10-bit fully differential successive approximation register analog-to-digital converter are fabricated by the TSMC 0.18 μm 1P6M 3.3 V process. The feature of the CVC is selectable for the detection points from 1 to 64, which is controlled by the digital codes of a field-programmable gate array (FPGA). It also has the embedded functions of crosstalk attenuation (CA) for cross-type capacitive sensors and a self-separated input signal for capacitive plantar pressure monitoring. The CA can effectively reduce parasitic capacitances and influences of the temperature and relative humidity of the environment: An M$\times$N array only requires M + N tracks of I/O ports to reduce detected complexity. The measured results shown on the display interfaces reveal the positions and amplitudes (voltage swings) of the corresponding capacitances. The conversion time for one capacitance is 0.4 ms, and the maximum conversion time for 64 capacitances is 25.6 ms. A handmade cross-type capacitive array and a cross-type capacitive plantar pressure sensor are used to demonstrate the detection system.

INDEX TERMS Acquisition module, display interface, capacitance-to-voltage converter, successive approximation register, analog-to-digital converter, capacitive sensor, capacitive plantar pressure sensor, crosstalk attenuation.

I. INTRODUCTION

Capacitive sensors play an important role in many fields, such as liquid-level measurements [1] and human body monitoring (e.g., respiration and plantar pressure). Given the simple structure of a capacitor, many features can be adopted. One method for capacitance measurement uses the overlapped-area variation of the conducted parallel plates to reveal the change in capacitance. Another [2] utilizes the distance variation between conducted parallel plates to illustrate capacitances. The proposed target in this study is the application of plantar pressure monitoring.

An abnormal plantar pressure can negatively influence gait, even affecting individuals' quality of life. The change of normal gait can induce a chain of adverse results, ranging from inflicting further high pressure onto a new location of the foot to placing individuals at a greater risk of imbalance and injury when walking. These results can also cause excessive changes in the degree of asymmetry between the plantar pressure of the left and right feet while walking, which further increases the risk of plantar injury. Dynamic measures, such as the plantar pressure distribution of the foot, can provide valuable information about the nature of individuals' gait. The information of plantar pressure can help identify the situation of plantar for curing.

Many types of multipoint plantar pressure monitoring are available, such as capacitive, piezoelectric, piezoresistive, and force-sensitive resistor sensors.

Capacitive sensors [3], [4] have a good AC response (variable force on the sensor) and DC response (stationary force on the sensor) due to good dielectric flexibility. Moreover, simple capacitor structures can be easily constructed and adjusted. However, they can be seriously influenced by temperatures, and the flatness of parallel plate must sufficiently obtain the same initial capacitance on different parallel plates. In addition, the output ports with many detection points on

The associate editor coordinating the review of this manuscript and approving it for publication was Cihun-Siyong Gong.

practical applications induce hardware cost. Methods [3]–[6] of multipoint capacitive plantar pressure sensor for monitoring the plantar pressure utilize the distance variation of two conductive parallel plates to reveal the capacitance.

Force-sensitive resistor sensors [7] are the mostly used sensors for plantar pressure monitoring. They have features of resistance varying inversely proportional to the pressure and are easy to gain and use (commercial products). However, the detection points hardly increase in a specific area.

Piezoelectric sensors [8], [9] have a good AC response but a poor DC response. Nevertheless, they do not require external power supply, and they are less sensitive to temperature. In addition, the output ports with many detection points on the practical applications induce hardware cost.

Piezoresistive sensors [10], [11] have good AC and DC responses. However, the quantity of hardware is high because of many output ports required.

To reach the goals of simple structure, easy implementation, and flexible application for plantar pressure monitoring, this study develops a simple capacitive $M \cdot N$ type array to achieve the functions of selectable detection points (1–64), $M + N$ tracks of the I/O ports, and a detection system with a crosstalk attenuation (CA). CA can effectively reduce parasitic capacitances of cross-type capacitive sensors and the influences of the relative humidity and temperature of the environment.

The remainder of this paper is as follows. Section II provides a detailed explanation of the proposed cross-type capacitive sensor. Section III describes the detection system. Section IV reveals the measurement results to demonstrate the achievement. Comparisons of similar approaches are described in Section V. Finally, Section VI concludes the study.

II. CROSS-TYPE CAPACITIVE SENSOR

This study develops a simple cross-type capacitive array (CCA) structure to demonstrate the implemented prototype, including the acquisition module and display interfaces. As shown in Fig. 1(a), the proposed CCA includes an SL (copper foil tape), two attaching layers (polypropylene), a top plate (copper foil tape), a dielectric (polyurethane), and a bottom plate (copper foil tape). The SL can isolate the noise of the environment and cover on the attaching layer. It is connected to the ground; hence, a large parasitic capacitance exists. Nevertheless, the SL is necessary to reduce the noises (V_{NOISE}) of the human body and environment, although the input signals of tracks are attenuated. The total parasitic capacitance with 64 cells in an array is 2 nF; thus, each parasitic capacitance connected to the ground is 31.25 pF (Fig.1(b)). In view of the influences of parasitic capacitances, virtual parasitic capacitors are added into the simulation by HSPICE, where the capacitances are set to be 80 pF for the tolerance of the distance between the SL and the top plate. The top and bottom plates are stuck on the backside of the attaching layer, and the dielectric is a flexible material between the top and bottom plates. All materials

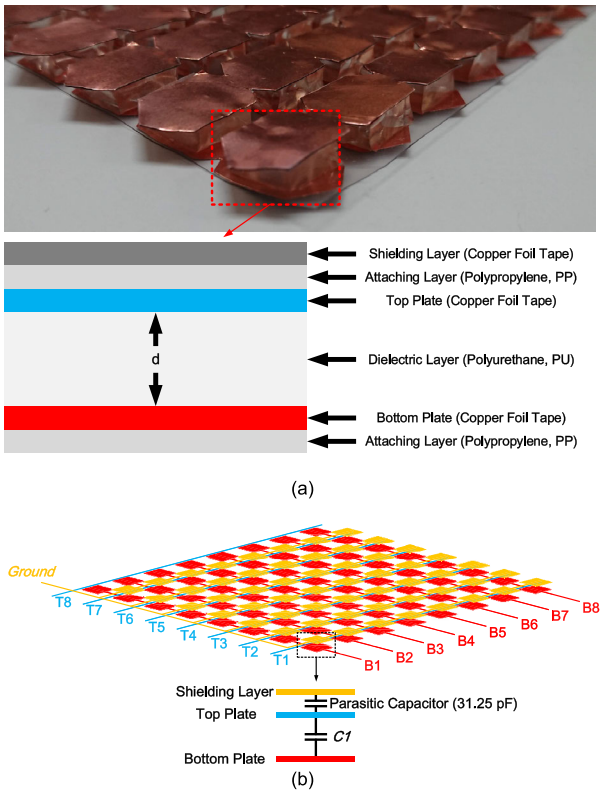

FIGURE 1. (a) Proposed CCA. (b) Parasitic capacitance contributed by SL.

are commercial products. Moreover, the characteristics of a capacitor can be easily presented as follows:

$$C = \varepsilon \frac{A}{d}. \tag{1}$$

The distance (d) is varied under the fixed area (A) and dielectric (ε); thus, it is inversely proportional to the capacitance (C). Therefore, if a force is applied on the top plate, then the distance between the conductive plates will decrease, and C is increased with the decrease of d. A capacitive 8×8 array is developed for the detection system to test the capability of the prototype acquisition module.

A. SINGLE CELL OF CROSS-TYPE CAPACITIVE ARRAY

A modeling cell of array simulated by COMSOL is shown in Fig. 2(a). The top plate connects to 3.3 V, whereas the bottom plate connects to 0 V. An electric field (red arrows) only exists between two plates, and the capacitance of ideal cell is 0.5814 pF, without the shielding layer (SL) and the fringe effect (FE), as shown in Fig. 2(b). The cell capacitance is 0.9838 pF. Fig. 2(c) shows the condition without the SL and with the FE. Evidently, the electric field is out of two plates with FE. Fig. 2(d) shows the electric field distribution of the cell with SL and FE, and the cell capacitance is 0.7902 pF. The SL adsorbs some electric field due to connecting to 0 V; thus, the electric field out of two plates is less than that in Fig. 2(c), and it can effectively reduce the FE.

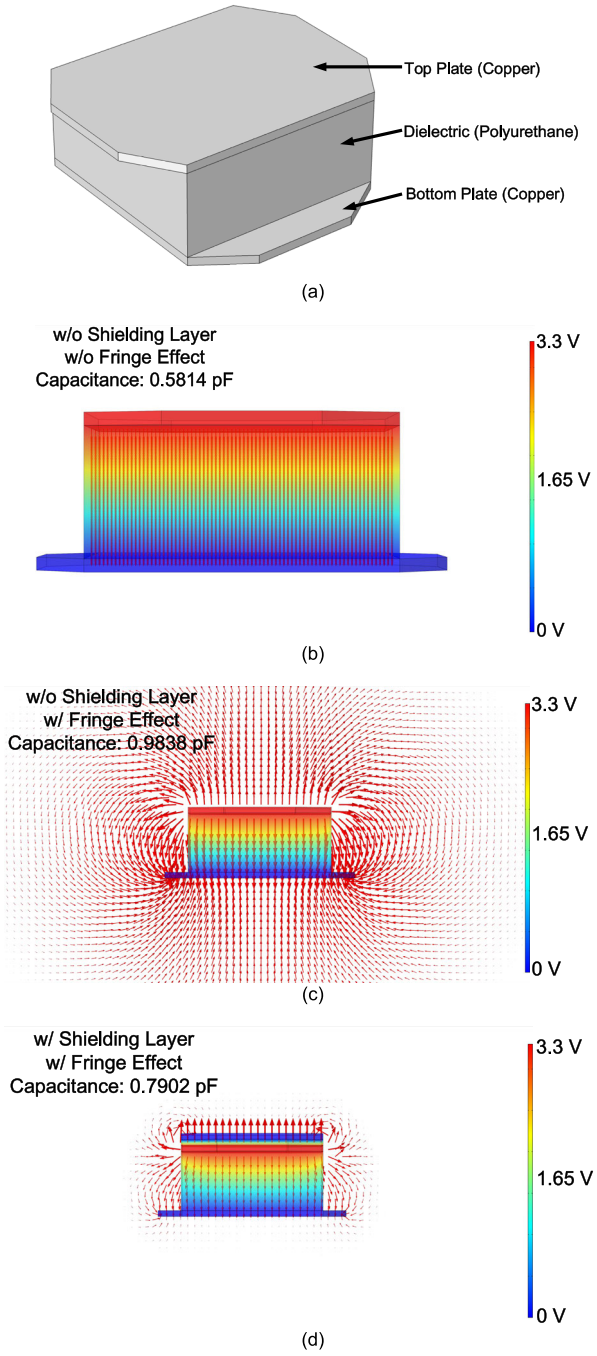

FIGURE 2. (a) Model of the cell of CCA. (b) Distributions of electric field of Fig. 2(a). (c) Distributions of electric field without SL and with FE. (d) Distributions of electric field with SL and FE.

Table 1 shows the capacitances of the aforementioned conditions in different distances. As shown in Fig. 3, the cell capacitances are closer to the ideal and are inversely proportional to distances (d) between two plates with FE and SL. The sensor is applied to detect plantar pressure; thus, relative variations of plantar pressure are important for this application.

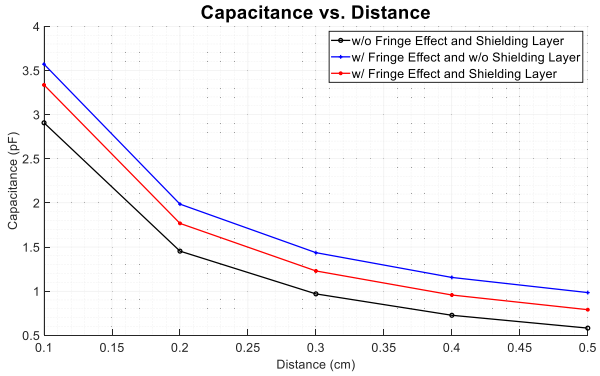

FIGURE 3. Effects of SL and FE to a single cell of CCA.

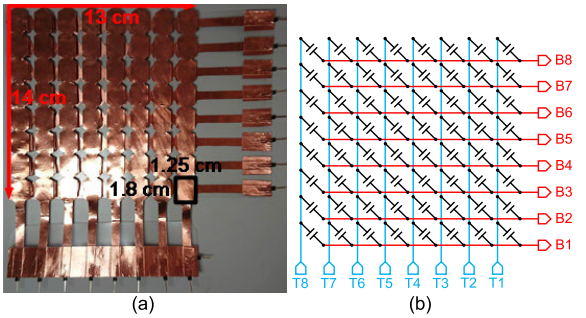

FIGURE 4. (a) Proposed CCA. (b) Equivalent model of Fig.4(a).

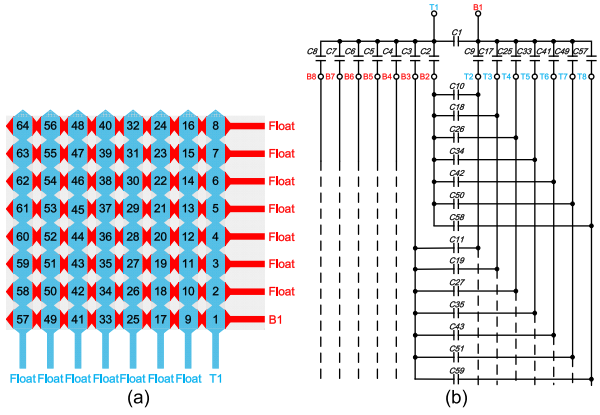

FIGURE 5. (a) Proposed CCA without a CA. (b) Equivalent model of Fig. 5(a).

B. CCA

1) ANALYSIS OF CA

Fig. 4(a) shows the proposed CCA with eight input (T1–T8) and eight output (B1–B8) channels. The equivalent model of the proposed capacitive sensor is shown in Fig. 4(b). On the basis of the structure, 64 capacitors per array are available. Therefore, scanning all unit cells will detect 64 variations in 64 coordinates. The size of the unit cell of the proposed capacitive sensor is 12.5 mm $\times$18 mm, and the entire size of the 64 cells is 130 mm $\times$140 mm.

TABLE 1. Capacitances for different distances in different conditions.

Simulated Condition	T: 293.15 K; V_{Top}:3.3 V; V_{Bot}: 0 V; V_{SL}: 0 V				
d (cm)	0.1	0.2	0.3	0.4	0.5
Capacitance w/o FE and SL (pF)	2.907	1.4535	0.969	0.7268	0.5814
Capacitance w/ FE and w/o SL (pF)	3.5711	1.9859	1.4361	1.1553	0.9838
Capacitance w/ FE and SL (pF)	3.3363	1.7678	1.229	0.9563	0.7901

T: Temperature
V_{Top}: Voltage of the top plate of the cell
V_{Bot}: Voltage of the bottom plate of the cell
V_{SL}: Voltage of shielding layer
d: Distance between two plates
FE: Fringe effect
SL: Shielding layer

TABLE 2. Measured parasitic capacitances with or without CA.

Simulated Condition	w/ FE; T: 293.15 K; w/ CA; V_{Top}: 1.65 V; V_{Bot}: 1.65V; V_{SL}: 0 V; V_{CA}: 1.65 V				
d (cm)	0.1	0.2	0.3	0.4	0.5
$C_{Parasitic}$ (pF)	1.2453	1.0157	0.8866	0.801	0.7418
C_{T_Top} (pF)	60.484	60.673	60.803	60.911	60.99
C_{T_Bot} (pF)	1.2453	1.0157	0.8866	0.801	0.7418
Simulated Condition	**w/ FE; T: 293.15 K; w/o CA; V_{Top}: 1.65 V; V_{Bot}: 1.65V; V_{SL}: 0 V**				
d (cm)	0.1	0.2	0.3	0.4	0.5
$C_{Parasitic}$ (pF)	22.951	13.426	9.9041	8.0582	6.9094
C_{T_Top} (pF)	78.866	70.785	67.905	66.466	65.615
C_{T_Bot} (pF)	22.951	13.426	9.9041	8.0582	6.9094

FE: Fringe effect
T: Absolute temperature
CA: Crosstalk attenuation
V_{Top}: Voltage of top plate of *C1*
V_{Bot}: Voltage of bottom plate of *C1*
V_{SL}: Voltage of shielding layer
V_{CA}: Voltage of crosstalk attenuation
d: Distance between two plates
$C_{Parasitic}$: Parasitic capacitance connects with *C1*
$C_{T\ Top}$: Total capacitance of top plate of *C1*
$C_{T\ Bot}$: Total capacitance of bottom plate of *C1*

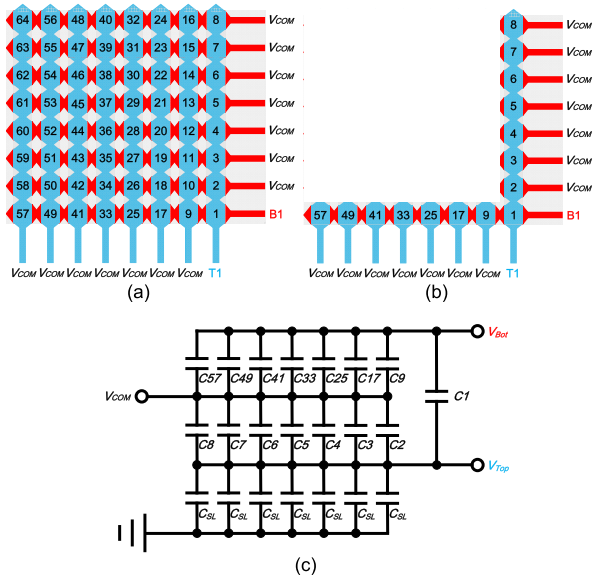

FIGURE 6. (a) Placement of the proposed CCA with the T1 and B1 turned on. (b) Two tracks are available when T1 and B1 are turned on. (c) Equivalent model of Fig. 6(b).

The proposed CCA is shown in Fig. 5(a). When the tracks of T1 and B1 are turned on, the other tracks will float and couple with all the capacitors of the CCA (Fig. 5(a)). Fig. 5(b) shows the equivalent model of the proposed CCA coupled with parasitic capacitances. Many parasitic capacitors are involved in *C1*. To solve this problem, the proposed capacitance-to-voltage converter (CVC) has an embedded function of controlling all floating tracks to connect with a common DC voltage ($V_{COM} = 1.65$ V; Fig. 6(a)). Then, only two tracks are available in the proposed CCA (Fig. 6(b)). *C1* connects with T1 and B1, and 14 capacitors and 7 shielding capacitors connect with two terminals to be the input and output loads, respectively (Fig. 6(c)).

Fig. 7(a) presents the model of the proposed CCA with the SL simulated by COMSOL Multiphysics. Fig. 7(b) shows the voltage distributions of CCA, in which *C1* has a large value of parasitic capacitance (4.3005 pF − 0.5814 pF = 3.7191 pF, where 4.3005 pF is the capacitance of the *C1* measured in Fig. 7(b) due to crosstalk, and 0.5814 pF is the capacitance of the *C1* measured in Table 1). To decrease the effect of crosstalk, the CA technique is utilized to reduce the influence. Moreover, V_{Top} and V_{Bot} of *C1* connect to V_{COM} to measure the parasitic capacitance coupled with *C1* (Fig. 7(c)). The voltage distributions of sensor with the CA is well-proportioned (Fig. 7(c)); however, the voltage distributions without the CA is nonuniform (Fig. 7(d)). Moreover, the differences between with and without CA are evident, as shown in Table 2. The smaller the distances are, the larger the parasitic capacitances will be without using the CA, as shown in Fig. 7(e). In addition, using the CA can have small and stable parasitic capacitances. Hence, the variations of parasitic capacitances can be neglected. Thus, using the CA can effectively reduce the parasitic capacitances

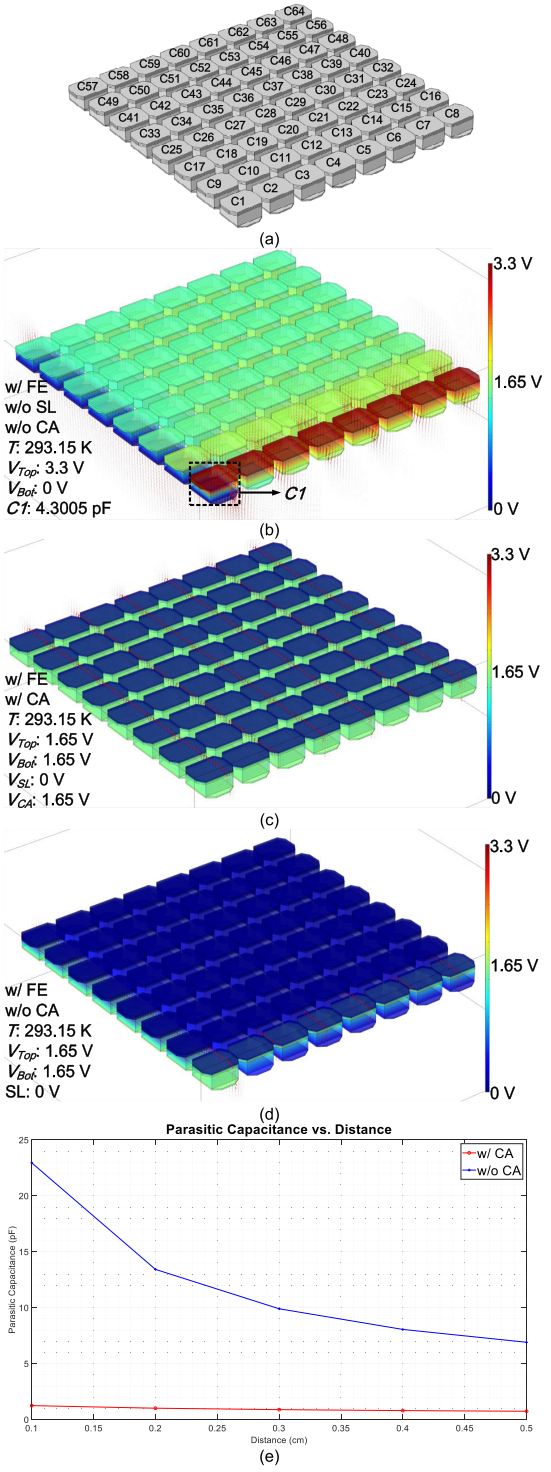

FIGURE 7. (a) Model of CCA by COMSOL Multiphysics. (b) Model of CCA without SL and CA. (c) Model of CCA with SL and CA. (d) Model of CCA with SL and without CA. (e) Difference of with and without CA.

coupling to the detection point. Fig. 8 shows an equivalent model of array with the CA, and the output of array measures the capacitance of *C1* with $C_{Parasitic}$, where $C_{Parasitic}$ is composed of 14 capacitances, and C_{T_Top} is a bypass capacitor.

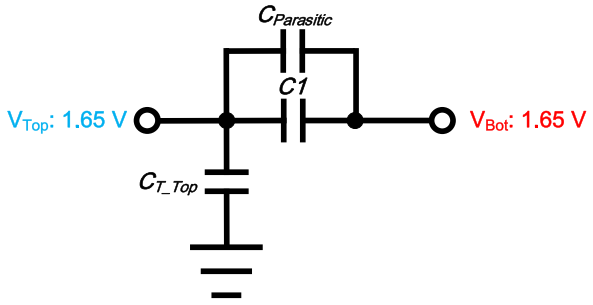

FIGURE 8. Equivalent model of CCA in Fig. 7(c).

This method eliminates 49 stray capacitors; however, 14 parasitic capacitors and 7 shielding capacitors are still attached to the terminals between the inputs (T1–T8) and outputs (B1–B8). The ideal situation is that all cells have the same initial capacitances and same pressures on the surface of the CCA. However, in the actual situation, the initial capacitances are different because the CCA is handmade and the pressures on the surface of CCA may be different. Thus, all detection points will have different stray capacitors connected to the input and output terminals.

2) INFLUENCES OF TEMPERATURE AND RELATIVE HUMIDITY

Fig. 9 shows the models of one CCA cell, which is simulated by COMCOL Multiphysics. C_{T_Top1} is the total capacitance of the top plate of one cell, C_{Cell} is the capacitance of one cell, C_{T_Top2} is the total capacitance of the top plate of *C1*, $C_{T\_Bottom2}$ is the total capacitance of the bottom plate of *C1*, and $C_{Parasitic}$ is the parasitic capacitance connected with the *C1* of CCA. $C_{T\_Bottom2}$ equals $C_{Parasitic}$ because the bottom plate only connects with $C_{Parasitic}$.

An equation of Reference [12] is used to simulate the effect of different temperatures and relative humidity of the environment by COMSOL Multiphysics, as shown as follows:

$$\varepsilon_{air} = \varepsilon_0 \cdot \left[1 + \frac{211}{T} \cdot \left(P + \frac{48 \cdot_S \cdot RH}{T}\right) \cdot 10^{-6}\right]. \quad (2)$$

where $\varepsilon_0 (8.85 \times 10^{-12} \mathrm{F/m})$ is the permittivity of the vacuum, T(K) is the absolute temperature, RH is the relative humidity (%), P(mmHg) denotes the air pressure, and P_S (mmHg) is the pressure of saturated water vapor at temperature T. The relative permittivity of air can be easily calculated by Reference [12], and P_S can be surveyed by Reference [13]. Finally, the parameters and equation are simulated by COMSOL Multiphysics, and the simulated results and figures are shown in Tables 3–6 and Figs. 10(a)-10(d). The results reveal that the variations are in an order of femtofarad, which can be neglected in our application.

C. CROSS-TYPE CAPACITIVE PLANTAR PRESSURE (CCPP) SENSOR

As shown in Fig. 11, the proposed CCPP sensor is an insole-type pressure sensor due to the flexible structure of CCA. Fig. 12(a) shows that an equivalent model of CCPP sensor is

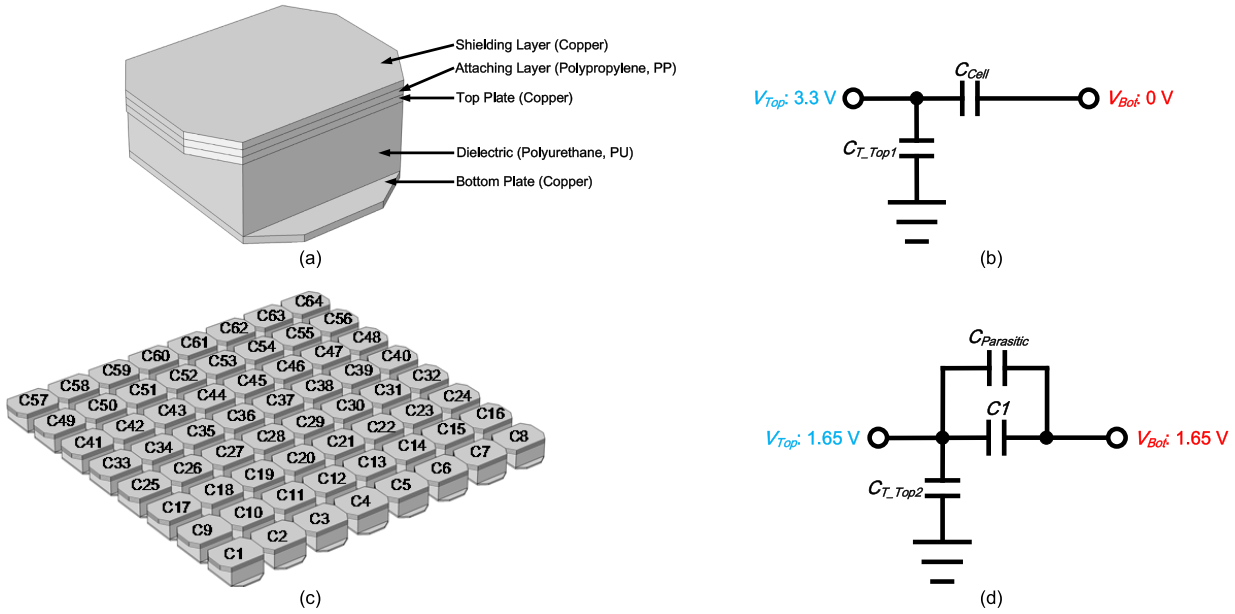

FIGURE 9. Models of proposed sensors. (a) Model of the single cell of CCA. (b) Equivalent model of Fig. 9(a). (c) Model of CCA. (d) Equivalent model of Fig. 9(c).

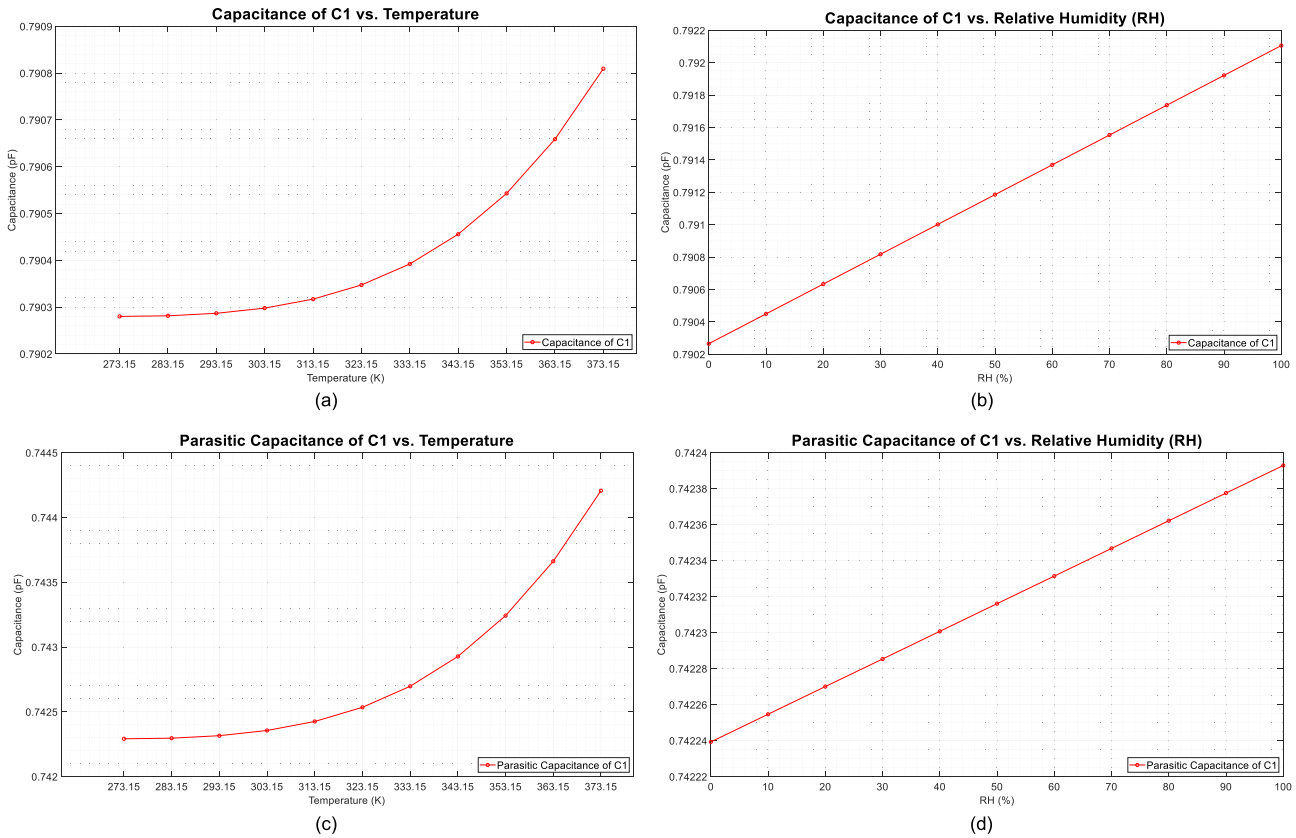

FIGURE 10. (a) Variations of capacitances of single cell with *T*. (b) Variations of capacitances of single cell with *RH*. (c) Variations of capacitances of CCA with *T*. (d) Variations of capacitances of CCA with *RH*.

similar to that in Fig. 4. Fig 12(b) shows the structure of the CCPP sensor, and Figs. 12(c) and 12(d) show its placements and connections. All detection points use the copper foil tape, each detection points are connected with conductive wires, and a commercial insole is used to be the dielectric (latex) of the CCPP sensor. Given this application, the detection system

TABLE 3. Capacitances of single cell with variations of *RH*.

Simulated Condition	*d*: 0.5 cm; *T*: 293.15 K; V_{Top}:3.3 V; V_{Bot}: 0 V; V_{SL}: 0 V										
***RH* (%)**	**0**	**10**	**20**	**30**	**40**	**50**	**60**	**70**	**80**	**90**	**100**
C_{T_Top1} (pF)	8.5085	8.5091	8.5096	8.5102	8.5108	8.5114	8.512	8.5125	8.5131	8.5137	8.5143
C_{Cell} (pF)	0.7903	0.7904	0.7906	0.7908	0.791	0.7912	0.7914	0.7916	0.7917	0.7919	0.7921

d: Distance between two plates
T: Temperature
V_{Top}: Voltage of top plate of cell
V_{Bot}: Voltage of bottom plate of cell
V_{SL}: Voltage of SL
RH: Relative humidity
C_{T_Top1}: Total capacitance of top plate of one cell
C_{Cell}: Capacitance of single cell

TABLE 4. Capacitances of single cell with variations of *T*.

Simulated Condition	*d*: 0.5 cm; *RH*: 50%; V_{Top}:3.3 V; V_{Bot}: 0 V; V_{SL}: 0 V										
***T* (K)**	**273.15**	**283.15**	**293.15**	**303.15**	**313.15**	**323.15**	**333.15**	**343.15**	**353.15**	**363.15**	**373.15**
P_S (mmHg)	**4.5979**	**9.2033**	**17.5514**	**31.8626**	**55.3921**	**92.6401**	**149.6073**	**234.0343**	**355.6418**	**526.4008**	**760.7201**
C_{T_Top1} (pF)	8.5085	8.5085	8.5085	8.5086	8.5086	8.5087	8.5089	8.5091	8.5093	8.5097	8.5102
C_{Cell} (pF)	0.7903	0.7903	0.7903	0.7903	0.7903	0.7903	0.7904	0.7905	0.7905	0.7907	0.7908

Ps: Pressure of saturated water vapor

TABLE 5. Total capacitances of two plates and parasitic capacitances of *C1* with variations of *RH*.

Simulated Condition	*d*: 0.5 cm; *T*: 293.15 K; V_{Top}:1.65 V; V_{Bot}: 1.65 V; V_{SL}: 0 V; V_{CA}: 1.65 V										
***RH* (%)**	**0**	**10**	**20**	**30**	**40**	**50**	**60**	**70**	**80**	**90**	**100**
C_{T_Top2} (pF)	61.015	61.0151	61.0151	61.0152	61.0152	61.0153	61.0154	61.0154	61.0155	61.0155	61.0156
C_{T_Bot2} (pF)	0.7422	0.7423	0.7423	0.7423	0.7423	0.7423	0.7423	0.7423	0.7424	0.7424	0.7424
$C_{Parasitic}$ (pF)	0.7422	0.7423	0.7423	0.7423	0.7423	0.7423	0.7423	0.7423	0.7424	0.7424	0.7424

C_{T_Top2}: Total capacitance of top plate of *C1*
C_{T_Bot2}: Total capacitance of bottom plate of *C1*
$C_{Parasitic}$: Parasitic capacitance connects to *C1*

TABLE 6. Total capacitances of two plates and parasitic capacitances of *C1* with variations of *T*.

Simulated Condition	*d*: 0.5 cm; *RH*: 50%; V_{Top}:1.65 V; V_{Bot}: 1.65 V; V_{SL}: 0 V; V_{CA}: 1.65 V										
***T* (K)**	**273.15**	**283.15**	**293.15**	**303.15**	**313.15**	**323.15**	**333.15**	**343.15**	**353.15**	**363.15**	**373.15**
P_S (mmHg)	**4.5979**	**9.2033**	**17.5514**	**31.8626**	**55.3921**	**92.6401**	**149.6073**	**234.0343**	**355.6418**	**526.4008**	**760.7201**
C_{T_Top2} (pF)	61.0152	61.0152	61.0153	61.0154	61.0157	61.0161	61.0168	61.0176	61.0188	61.0204	61.0225
C_{T_Bot2} (pF)	0.7423	0.7423	0.7423	0.7424	0.7424	0.7425	0.7427	0.7429	0.7432	0.7437	0.7442
$C_{Parasitic}$ (pF)	0.7423	0.7423	0.7423	0.7424	0.7424	0.7425	0.7427	0.7429	0.7432	0.7437	0.7442

is used to react with the relative variations of each cell of the CCPP sensor. The data of the detection system can be used for further analyses of the plantar pressure.

III. DETECTION SYSTEM

Fig. 13 demonstrates the block diagram of the entire detection system, which comprises a low-dropout regulator that outputs 3.3 V for the entire system (TPS71701 with power supplied by a 3.7 V Li-ion battery), the proposed CCA and CCPP sensor, the proposed CVC, the proposed 10-bit fully differential successive approximation register analog-to-digital converter (SAR ADC), a clock generator, a single-to-differential amplifier (SDA), a field-programmable gate array (FPGA), and a personal computer (PC).

The commercial chip (oscillator LTC6900) is used as the clock generator, and another chip (ADC driver, AD8137) is applied to convert the input signal into a differential output. The FPGA (Altera, DE0-nano) is adopted to divide the clock

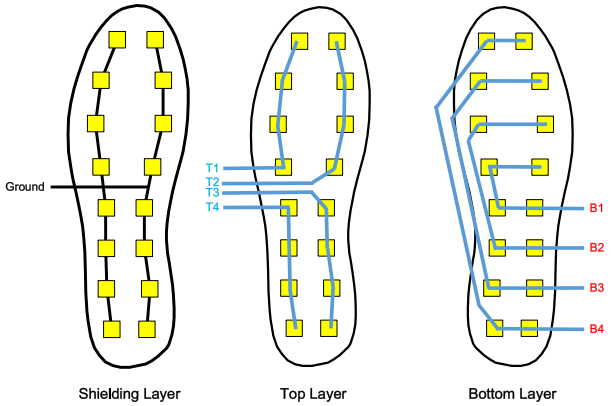

FIGURE 11. Connections and placements of the proposed CCPP sensor.

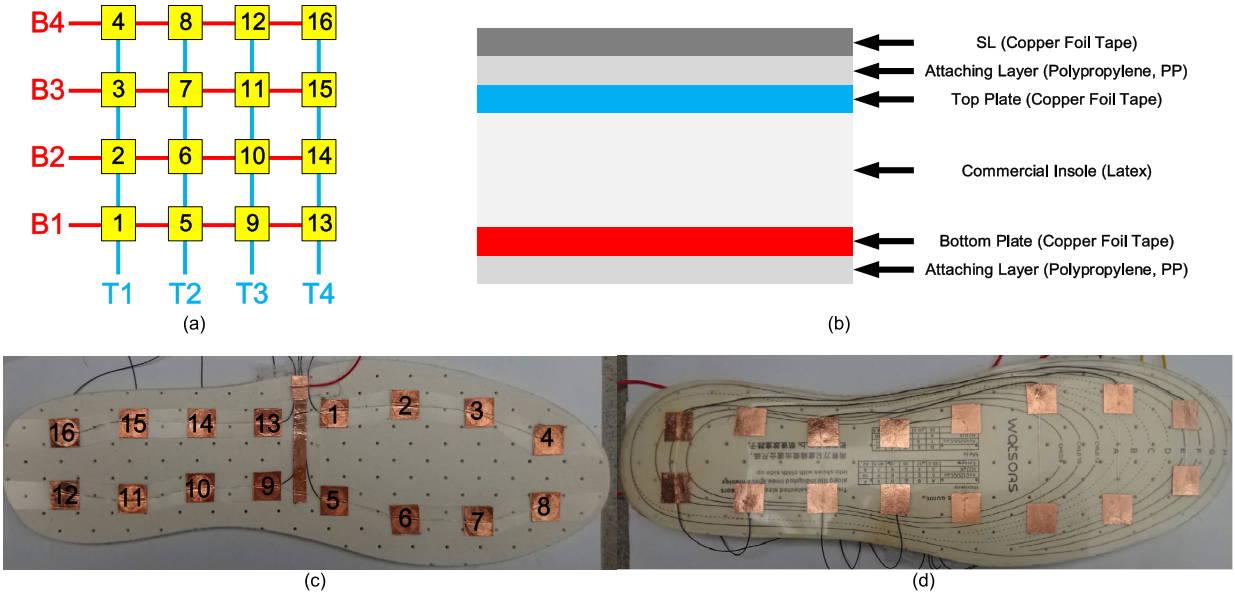

FIGURE 12. (a) Equivalent model of Fig. 11. (b) Structure of CCPP sensor. (c) Top view of CCPP sensor. (d) Bottom view of CCPP sensor.

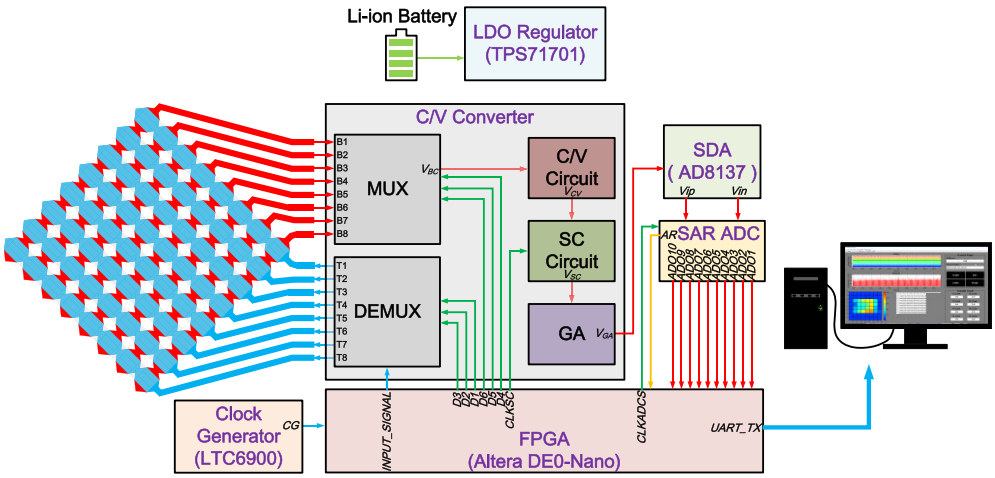

FIGURE 13. Block diagram of the entire detection system.

of the clock generator, collect data from the outputs of the 10-bit fully differential SAR ADC, and transmit the data to the PC. The CVC and the 10-bit fully differential SAR ADC are fabricated by the TSMC 0.18 μm 1P6M 3.3 V process.

Fig. 14 shows the timing diagram of the entire detection system. The clock generator generates the clock (*CG*) into the FPGA. Then, the FPGA divides *CG* into nine clocks (i.e., *INPUT_SIGNAL*, *CLKADCS*, *CLKSC*, and *D1–D6*). The clock (*INPUT_SIGNAL*) senses the cell capacitances of the proposed capacitive sensor. The clocks (*D1–D3*) control the demultiplexer (DEMUX) to separate the input signal into the determined channels (T1–T8). Subsequently, the clocks (*D4–D6*) control the multiplexer (MUX) to collect the outputs of the proposed capacitive sensor into the input (V_{BC}) of the capacitance-to-voltage (CV) circuit. The CV circuit then amplifies V_{BC} as V_{CV}. The switched-capacitor (SC) circuit is used to sample V_{CV}, and the gain stage (GA) will amplify V_{CV}, which outputs V_{GA} and is transformed to the differential signals (*Vip* and *Vin*) by the SDA. The differential signal will be transformed into 10-bit digital codes by the 10-bit fully differential SAR ADC. Finally, the digital codes are transmitted to the PC through the universal asynchronous receiver/transmitter (UART) of the FPGA.

The conversion time is controlled by *CLKSC*, as shown in Fig. 14. The fastest controlling clock (*D4*) of the CCA is 1.25 kHz (0.8-ms); thus, each cell only needs a half cycle (0.4 ms) of *D4* to be converted. Moreover, the conversion time for one capacitance is 0.4 ms (0.2 ms for the capacitance conversion to voltage and 0.2 ms for the prototype acquisition module to reset). The maximum conversion time for 64 capacitances is 25.6 ms (0.4 ms multiplied by 64).

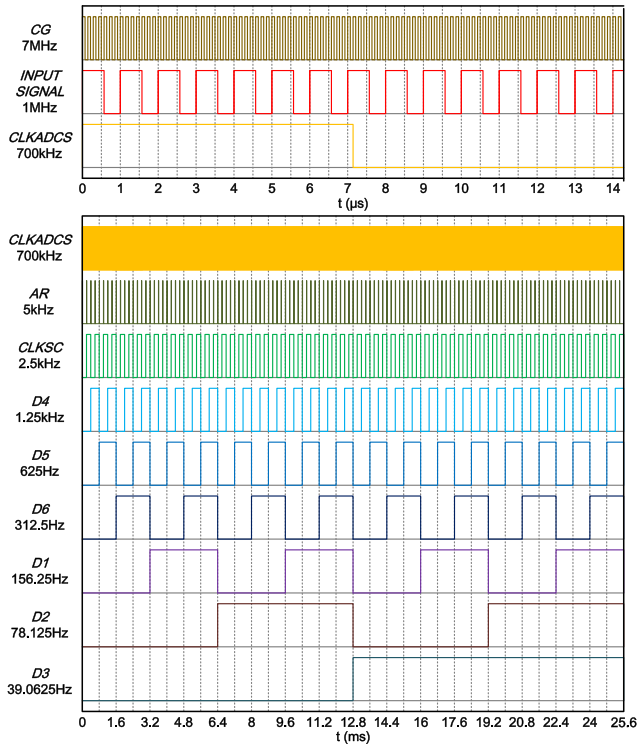

FIGURE 14. Timing diagram of the entire detection system.

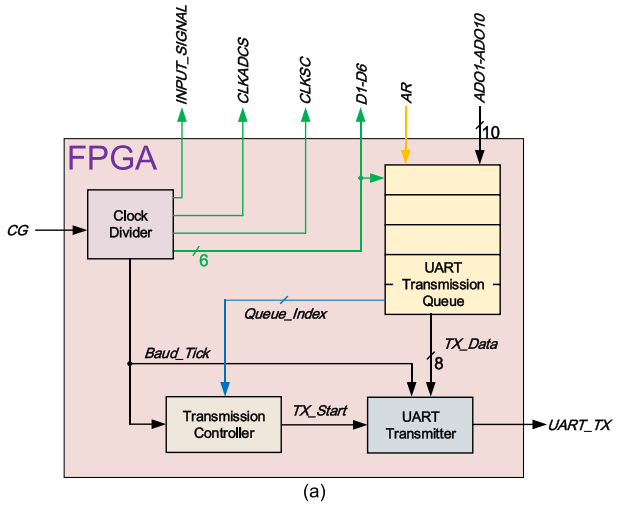

UART Transmission Format Configuration

HEADER 0xF				0xF			
D3	D2	D1	D6	D5	D4	ADO10	ADO9
ADO8	ADO7	ADO6	ADO5	ADO4	ADO3	ADO2	ADO1

(b)

FIGURE 15. (a) Structure of the FPGA. (b) Format of *UART_TX*.

A. FPGA

Fig. 15(a) shows the structure of the FPGA digital core. The UART format is N-8-1, and the baud rate is 230400 bit/s in the proposed structure. When CG is inputted into the clock divider, the input (*INPUT_SIGNAL*) and controlling signals (*CLKADCS*, *CLKSC*, and *D1–D6*) will be produced. *Baud_Tick* configures the baud rate of the UART. The outputs (*ADO10–ADO1*) are applied in the UART transmission queue, whereas the acquisition signal (*AR*) is at the positive edge. The signal (*Queue_Index*) will enable the transmission controller to trigger the UART transmitter to transmit the data of the UART transmission queue. Fig. 15(b) shows the format configuration of the UART containing three packets, namely, the header, address codes (*D1–D6*), and digital codes (*ADO10–ADO1*).

B. CVC

In this study, a conventional two-stage operational amplifier (OPA) [14] is utilized in the entire analog block. Table 7 presents the OPA specification. The CVC comprises the DEMUX, MUX, CV circuit, SC circuit, and GA. Fig. 16 shows the detailed circuits. The resistors are external components for adjusting the resistances to fit the required gain for the proposed CCA and CCPP sensor.

1) DEMUX/MUX

DEMUX is used to separate the input signal into the determined channel (controlled by digital signals *D1–D3*) on the top plate, and the output signals of the determined channel (controlled by digital signals *D4–D6*) on the bottom plate are converged into the output (bottom convergence, V_{BC}) of the MUX, as shown in Fig. 17. The transmission gates (TGs) are a dual-direction circuit controlled by the MUX/DEMUX.

TABLE 7. Simulation of two-stage OPA.

Parameter	Pre-sim, TT Corner, 25 °C, 3.3V
Gain	72.4 dB
Gain Bandwidth Product	158 MHz
Phase Margin	66°
Power Consumption	0.871 mW
Common Mode Rejection Ratio	71dB
Power Supply Rejection Ratio	69 dB
Input Common Mode Range	0.34–2.55 V
Output Swing	0.48–2.75 V
Slew Rate	SR+: 78.5 V/μs; SR-: 292.5 V/μs

2) CV CIRCUIT

Fig. 16(a) illustrates the CV circuit with $C_{ARRAY} = C_{REF} = C$ and R_1. V_{NOISE} is the noise coupled by the SL (if an object with static electricity is placed on the capacitive sensor). $V_{BC} + V_{NOISE}$ is the noise coupled by the capacitive sensor with V_{BC}. Then, the equation is presented as follows:

$$V_{CV} = R_1 \times sC \times [V_{NOISE} - (V_{BC} + V_{NOISE})], \quad (3)$$

$$V_{CV} = -R_1 \times sC \times V_{BC}. \quad (4)$$

If R_1, s, and V_{BC} are fixed, then C will be proportional to V_{CV}. Given this feature, the force on the proposed capacitive

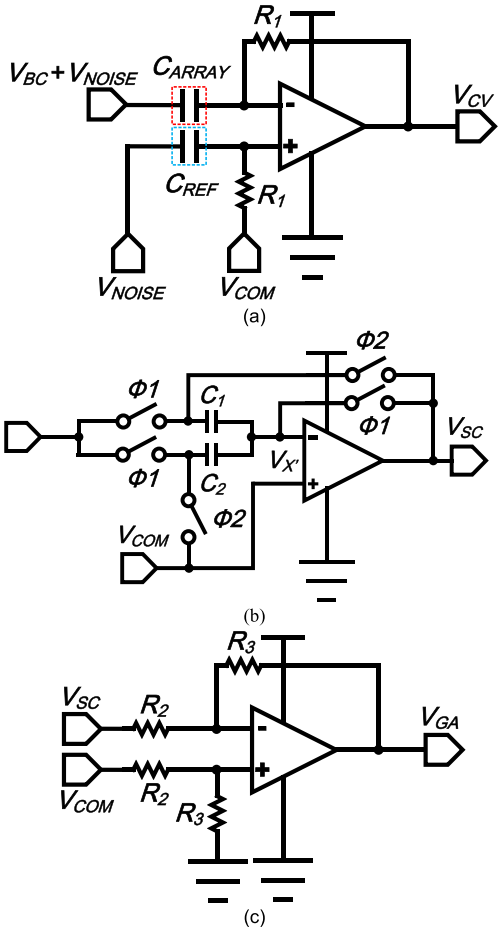

FIGURE 16. (a) Schematic of the CV circuit. (b) Schematic of the SC circuit. (c) Schematic of the GA.

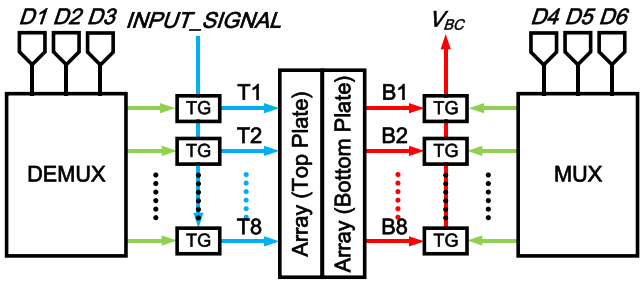

FIGURE 17. Controlling method of MUX/DEMUX.

sensor will be proportional to the magnitude of V_{CV}. In an actual situation, C_{ARRAY} and C_{REF} are not equal because C_{ARRAY} is varied by the distance (d) and C_{REF} is fixed.

3) SC CIRCUIT

Fig. 16(b) shows the SC circuit. The amplifier is connected with two capacitors ($C_1 = C_2 = C$). In the sampling mode ($\phi 1$ on and $\phi 2$ off), a virtual ground is established at the node (V_X), and the voltage across C_1 and C_2 is allowed to track V_{CV}. The total charge on C_1 and C_2 is equal to 2 CV_{CV}. Given that the voltage across C_2 approaches zero in the amplification mode ($\phi 1$ off and $\phi 2$ on), the final voltage across C_1 results in an output voltage (V_{SC}) approximately equal to 2 CV_{CV}.

TABLE 8. Measured voltages of with and without the CA.

No.	V_{cap} (V)	w/ CA (V)	w/o CA (V)	No.	V_{cap} (V)	w/ CA (V)	w/o CA (V)
1	0.304	0.702	3.108	33	0.075	0.173	1.636
2	0.294	0.684	3.072	34	0.072	0.160	1.586
3	0.284	0.666	3.034	35	0.069	0.148	1.535
4	0.274	0.648	2.995	36	0.067	0.136	1.484
5	0.263	0.630	2.955	37	0.065	0.125	1.432
6	0.254	0.612	2.915	38	0.063	0.115	1.380
7	0.243	0.594	2.875	39	0.061	0.106	1.327
8	0.234	0.557	2.834	40	0.059	0.098	1.274
9	0.224	0.558	2.772	41	0.057	0.094	1.214
10	0.215	0.541	2.730	42	0.056	0.087	1.160
11	0.205	0.523	2.689	43	0.054	0.081	1.108
12	0.196	0.506	2.647	44	0.053	0.076	1.051
13	0.187	0.488	2.604	45	0.051	0.071	0.996
14	0.179	0.471	2.561	46	0.050	0.067	0.940
15	0.171	0.453	2.518	47	0.049	0.063	0.883
16	0.163	0.436	2.474	48	0.048	0.059	0.827
17	0.156	0.424	2.413	49	0.047	0.059	0.776
18	0.148	0.407	2.369	50	0.046	0.056	0.709
19	0.141	0.390	2.324	51	0.045	0.053	0.651
20	0.134	0.373	2.279	52	0.044	0.051	0.592
21	0.128	0.356	2.233	53	0.043	0.049	0.533
22	0.122	0.339	2.187	54	0.042	0.047	0.474
23	0.116	0.322	2.454	55	0.041	0.045	0.414
24	0.111	0.306	2.408	56	0.041	0.043	0.354
25	0.105	0.292	2.035	57	0.040	0.043	0.291
26	0.101	0.276	1.988	58	0.040	0.042	0.231
27	0.096	0.260	1.940	59	0.039	0.041	0.174
28	0.092	0.244	1.892	60	0.039	0.040	0.126
29	0.088	0.228	1.843	61	0.038	0.039	0.091
30	0.084	0.213	1.794	62	0.038	0.038	0.067
31	0.081	0.198	1.744	63	0.037	0.037	0.053
32	0.078	0.183	1.695	64	0.037	0.036	0.043

4) GA

Fig. 16(c) demonstrates the GA by using the superposition theorem, which can be expressed as follows:

$$V_{GA} = \frac{R_3}{R_2}(V_{COM} - V_{SC}). \tag{5}$$

Therefore, V_{GA} is proportional to V_{SC} with the gain of R_3/R_2.

C. CA AND SELF-SEPARATED INPUT SIGNAL

As shown in Fig. 18(a), the block diagram of CA consists of TGs, inverters (INVs), the DEMUX, the MUX, and the CCA. In addition, all circuits are on chip except the CCA. *INPUT_SIGNAL* connects to a terminal of the TGs, and the TGs are controlled by the DEMUX (controlled by digital codes *D1–D3*). Moreover, *INPUT_SIGNAL* will be separated into several segments by controlling the DEMUX through the digital codes (*D1–D3*), which is called a "self-separated input signal" (Fig. 18(a)). The external commercial ICs of References [8]–[11] can also be used to separate the input

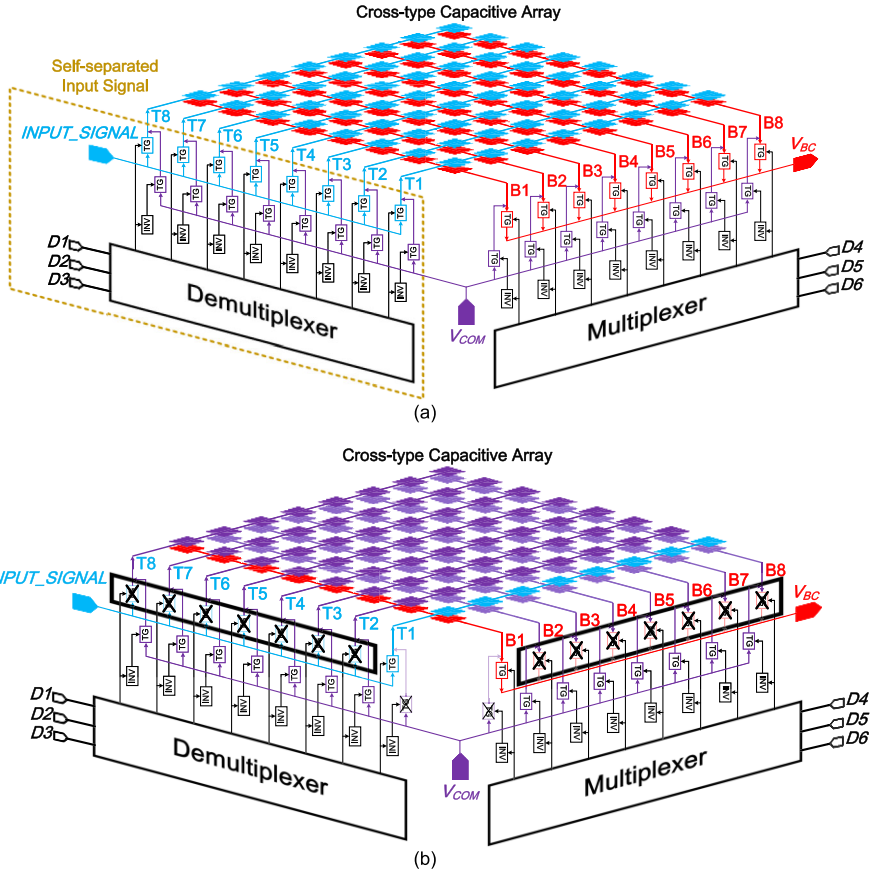

FIGURE 18. Introduction of CA function. (a) Block diagram of the CA with a CCA. (b) Example for the procedure of CA.

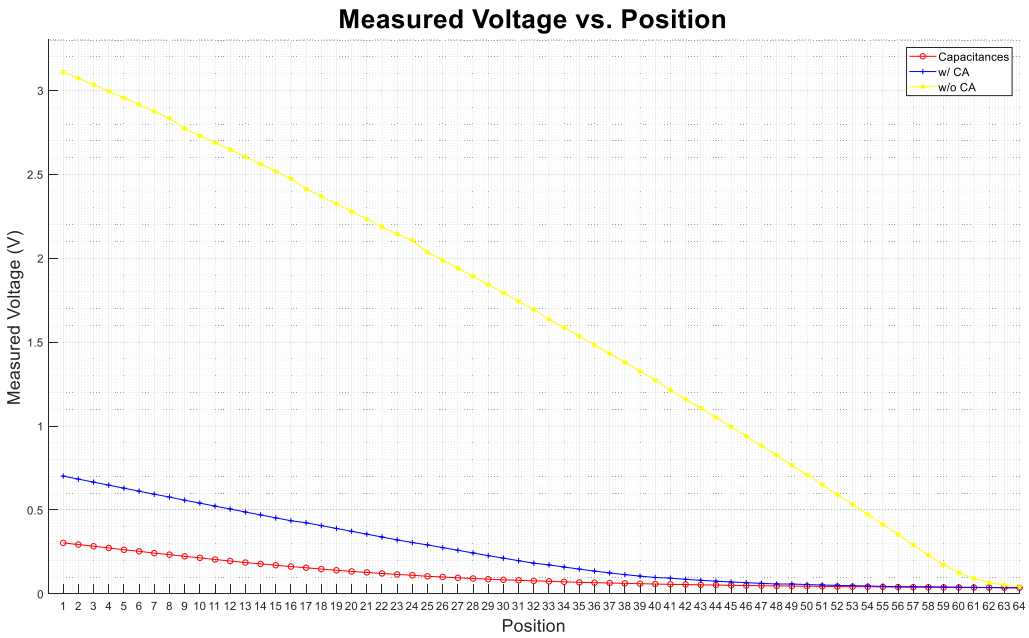

FIGURE 19. Deviation with or without the CA circuits under different positions.

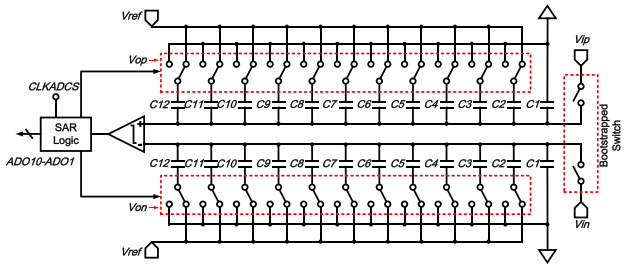

FIGURE 20. Schematic of the proposed 12-bit fully differential SAR ADC.

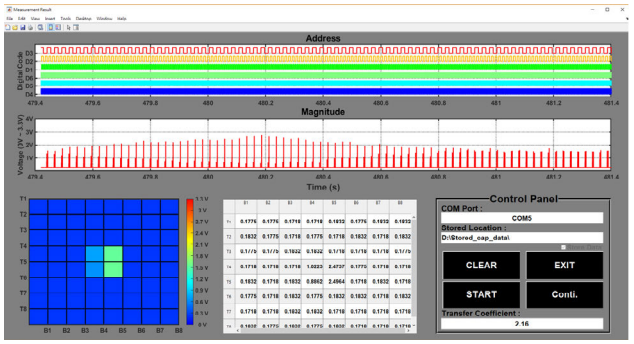

FIGURE 21. GUI of the proposed display interface by MATLAB.

signal; however, the complexity and area of modules will be higher. V_{BC} is used to collect the variations of the CCA controlled by the MUX through digital codes (*D4–D6*).

The procedure of CA is shown in Fig. 18(b). For instance, the detection coordinate (T1, B1) is the current target; therefore, the input channel (T1) and the output channel (B1) will be turned on. Then, other channels (black boxes) will be turned off and connected to V_{COM}. The following procedure has been described in Section II, Subsection B1.

To verify the CA, HSPICE is used to simulate the effect. A CCA is composed of the embedded capacitors of HSPICE, as shown in Fig. 4(b). Sixty-four capacitances (from 4 pF to 0.0625 pF) of the CCA decreased by a step of 0.0625 pF. A virtual CVC (functions as self-designed CVC) is utilized to convert capacitances to voltages. Table 8 shows the measured voltages (V_{cap}) of the virtual CVC with or without the function of CA. The deviation between with and without CA illustrates the decreasing quantity of the parasitic capacitances, as shown in Table 9. Fig. 19 indicates that the 64 capacitances range from 4 pF to 0.0625 pF.

D. 10-BIT FULLY DIFFERENTIAL SAR ADC

Fig. 20 shows the block diagram of the proposed design of 12-bit SAR ADC, which consists of bootstrapped switches [15], a dynamic comparator, capacitive digital-to-analog converters, and SAR control logic. The entire circuit is a typical 12-bit fully differential SAR ADC, and a monotonic switching procedure [16] is selected for this circuit. Due to the application, only the maximum 10-bit are used to digitalize the CVC output.

TABLE 9. Absolute error of with and without the CA.

No.	w/ CA (V)	w/o CA (V)	No.	w/ CA (V)	w/o CA (V)
1	0.398	2.804	**33**	0.098	1.561
2	0.390	2.778	**34**	0.088	1.514
3	0.382	2.750	**35**	0.079	1.466
4	0.374	2.721	**36**	0.069	1.417
5	0.367	2.692	**37**	0.060	1.367
6	0.358	2.661	**38**	0.052	1.317
7	0.351	2.632	**39**	0.045	1.266
8	0.343	2.600	**40**	0.039	1.215
9	0.334	2.548	**41**	0.037	1.157
10	0.326	2.515	**42**	0.031	1.104
11	0.318	2.484	**43**	0.027	1.054
12	0.310	2.451	**44**	0.023	0.998
13	0.301	2.417	**45**	0.020	0.945
14	0.292	2.382	**46**	0.017	0.890
15	0.282	2.347	**47**	0.014	0.834
16	0.273	2.311	**48**	0.011	0.779
17	0.268	2.257	**49**	0.012	0.719
18	0.259	2.221	**50**	0.010	0.663
19	0.249	2.183	**51**	0.008	0.606
20	0.239	2.145	**52**	0.007	0.548
21	0.228	2.105	**53**	0.006	0.490
22	0.217	2.065	**54**	0.004	0.431
23	0.206	2.028	**55**	0.003	0.372
24	0.195	1.995	**56**	0.002	0.313
25	0.187	1.930	**57**	0.003	0.251
26	0.175	1.887	**58**	0.002	0.191
27	0.164	1.844	**59**	0.002	0.135
28	0.152	1.800	**60**	0.001	0.087
29	0.140	1.755	**61**	0.001	0.053
30	0.129	1.710	**62**	0	0.029
31	0.117	1.663	**63**	0	0.016
32	0.105	1.617	**64**	-0.001	0.006

The operation can be simply divided into two phases, namely, sampling and conversion. Given that the operation is a fully differential structure, the operation of positive and negative sides is complementary. Hence, only the positive side of the operation is described below.

First, at the sampling phase, all the bottom plates of capacitors are reset to *Vref*, and the input signal (*Vip*) is sampled on the top plates of capacitors (V_+) through the bootstrapped switches.

Second, the operation enters the conversion phase, where the comparator directly works on the first comparison without switching any capacitors after the bootstrapped switches are turned off. The comparator determines if V_+ is larger than V_-. If so, then the most significant bit (MSB) is 1, and the bottom plate of the largest capacitor at the positive side is switched to the ground, resulting in $V_+(n) = V_+(n-1) - Vref/2$. Simultaneously, the bottom plate of the largest capacitor at the negative side remains unchanged, resulting in $V_-(n) = V_-(n-1)$. Otherwise, the MSB is 0, and the bottom plate of the largest capacitor at the positive side remains unchanged, resulting in $V_+(n) = V_+(n-1)$. Meanwhile, the bottom plate of the largest capacitor at the negative side is switched to *Vref*, resulting in $V_-(n) = V_-(n-1) - Vref/2$. This procedure will be executed iteratively until the least significant bit (LSB) is determined.

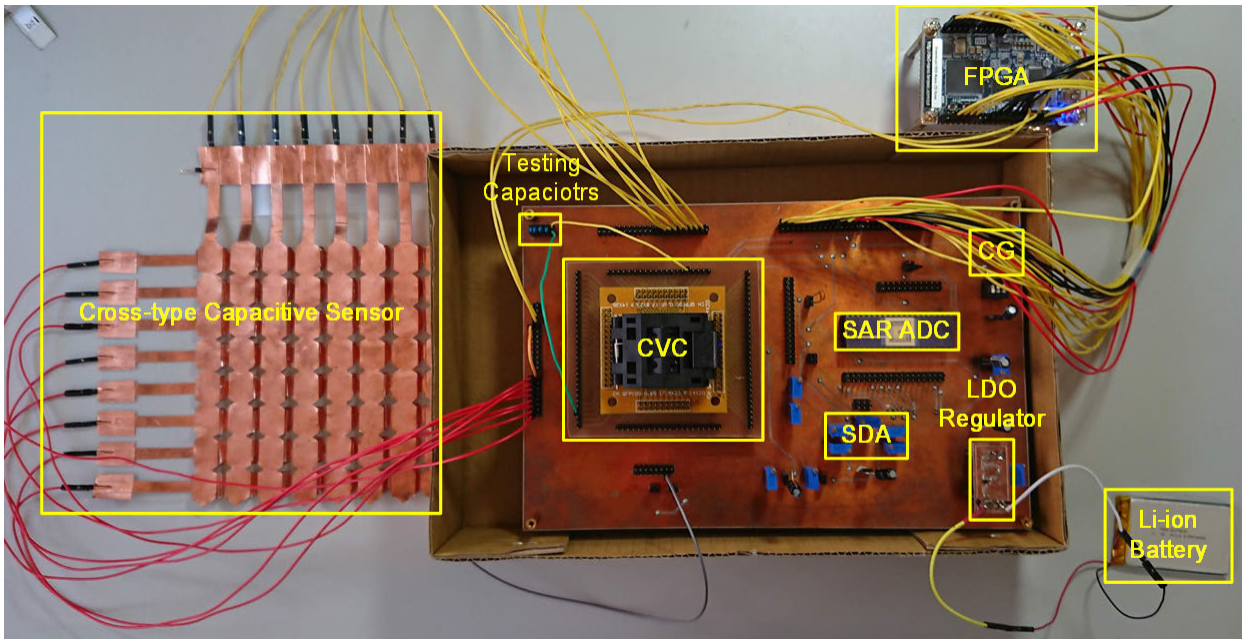

FIGURE 22. Entire detection system with the proposed CCA.

TABLE 10. Measured capacitances of commercial capacitors with an LCR meter.

Mark	Group 1	Group 2	Group 3	Group 4	Group 5	Group 6	Group 7	Group 8	Group 9
1 pF	1.177 pF	1.242 pF	1.105 pF	1.141 pF	1.276 pF	1.29 pF	1.27 pF	1.231 pF	1.278 pF
2 pF	2.246 pF	2.268 pF	2.063 pF	2.304 pF	2.366 pF	1.772 pF	2.248 pF	2.365 pF	2.295 pF
3 pF	3.045 pF	2.738 pF	2.739 pF	3.044 pF	3.136 pF	3.145 pF	3.378 pF	3.202 pF	3.133 pF
4 pF	3.923 pF	4.063 pF	4.187 pF	4.167 pF	4.021 pF	4.234 pF	4.14 pF	4.142 pF	4.07 pF
5 pF	5.405 pF	4.946 pF	5.244 pF	5.326 pF	5.34 pF	5.437 pF	5.377 pF	5.337 pF	5.368 pF

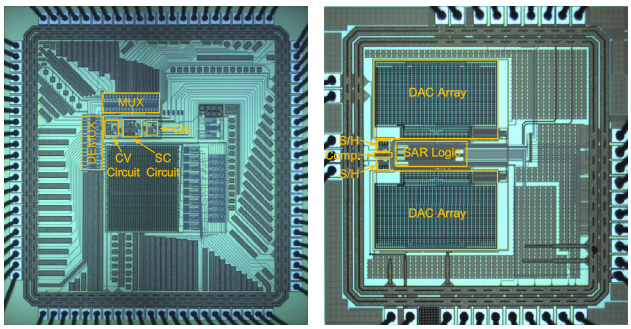

(a) (b)

FIGURE 23. Chip photographs. (a) All circuits of the proposed CVC. (b) All circuits of the proposed 12-bit fully differential SAR ADC.

E. DISPLAY INTERFACE

As shown in Fig. 21, the display interfaces are implemented in the graphical user interface (GUI) of MATLAB, and the measured results are the real-time display. The GUI has diagrams for the address (top), amplitude (media), and color temperature map (bottom). The capacitance table corresponds to the color temperature map. When the color is warm, the capacitance is large. The icon (START) will trigger all the diagrams to display, the icon (PAUSE) will force all the procedures to suspend and hold, the icon (CLEAR) will clean all the diagram and data, and the icon (EXIT) will close the GUI.

IV. MEASUREMENT

As shown in Fig. 22, the entire detection system includes the proposed CCA, prototype acquisition module, and FPGA. Fig. 23 shows the chip photographs of the CVC and 10-bit fully differential SAR ADC.

A. CVC

Fig. 24 presents a man pressing one cell on the proposed CCA, and the measured result is displayed on the screen of an oscilloscope (KEYSIGHT DSO-S 054A). The coordinate (T2, B8) of the pressed point can be easily realized due to the digital codes (*D1*, *D3*, and *D4*). The detection range of the prototype acquisition module is set to 0–6 pF. The demonstrated procedure is described as follows.

Initially, five testing capacitors (commercial capacitors, capacitances = 1–5 pF) are used to standardize the prototype acquisition module. These testing capacitors are then applied

TABLE 11. Measured voltages of commercial capacitors with the prototype acquisition module.

Mark	Group 1	Group 2	Group 3	Group 4	Group 5	Group 6	Group 7	Group 8	Group 9
1 pF	0.697 V	0.705 V	0.75 V	0.841 V	0.848 V	0.735 V	0.773 V	0.795 V	0.735 V
2 pF	1.348 V	1.394 V	1.371 V	1.379 V	1.515 V	1.273 V	1.409 V	1.485 V	1.47 V
3 pF	1.848 V	1.955 V	1.932 V	1.894 V	2.023 V	1.992 V	2.098 V	2.083 V	1.939 V
4 pF	2.508 V	2.455 V	2.386 V	2.5 V	2.47 V	2.614 V	2.5 V	2.515 V	2.553 V
5 pF	3.076 V	3.038 V	3.038 V	3.023 V	3.061 V	3.167 V	3.061 V	3.114 V	3.03 V

TABLE 12. Relative errors of commercial capacitors according to linear equation (6).

Mark	Group 1	Group 2	Group 3	Group 4	Group 5	Group 6	Group 7	Group 8	Group 9
1 pF	18.37%	23.16%	1.61%	−8.53%	1.29%	21.57%	12.6%	5.52%	20.44%
2 pF	5.03%	2.19%	−5.32%	5.06%	−2.72%	−11.7%	0.1%	−0.6%	−2.46%
3 pF	0.92%	−14.58%	−13.46%	−1.75%	−5.68%	−3.83%	−2.28%	−6.66%	−1.39%
4 pF	−6.09%	−0.52%	5.66%	0.09%	−2.18%	−2.97%	−0.56%	−1.14%	−4.38%
5 pF	4.43%	−3.19%	2.65%	4.79%	3.7%	1.9%	4.42%	1.8%	5.36%

TABLE 13. Relative errors of table 10 according to linear equation (6).

Mark	Group 1	Group 2	Group 3	Group 4	Group 5	Group 6	Group 7	Group 8	Group 9
1 pF	−15.52%	−18.81%	−1.58%	9.33%	−1.27%	−17.74%	−11.19%	−5.23%	−16.97%
2 pF	−4.78%	−2.14%	5.62%	−4.82%	2.79%	13.25%	−0.1%	0.61%	2.53%
3 pF	−0.91%	17.07%	15.55%	1.78%	6.02%	3.99%	2.33%	7.13%	1.41%
4 pF	6.48%	0.52%	−5.35%	−0.09%	2.23%	3.06%	0.56%	1.15%	4.58%
5 pF	−4.24%	3.29%	−2.58%	−4.57%	−3.57%	−1.86%	−4.23%	−1.77%	−5.09%

to an LCR meter (KEYSIGHT E4980AL) to measure the actual capacitances of the testing capacitors. Finally, the proposed cross-type capacitive sensor is connected to the prototype acquisition module.

Fig. 25 illustrates the measurements of the testing capacitors. The capacitances of the testing capacitors are 1.177, 2.246, 3.045, 3.923, and 5.405 pF for Group 1, and the testing capacitors are individually connected to one channel, as shown in Fig. 25(a)–25(e), respectively. Then, the corresponding voltages are measured and the linear equation is calculated using MATLAB. Table 10 presents the measured capacitances (measured by the LCR meter) of the commercial capacitors, which are marked 1–5 pF, and they are separated into nine groups. Table 11 lists the corresponding voltages of the measured capacitances with the prototype acquisition module.

By using the function of the curve fitting by MATLAB, the linear equation is

$$Capacitance = 1.7576 \times Voltage - 0.2307. \quad (6)$$

After calculation, Table 12 shows the relative errors of the commercial capacitors relative to the linear equation, and Fig. 26 plots the data and linear Equation (6). The data of the nine groups have the same trend. Measured results will be polluted because the environment of measurement has different noises, such as instrumentation, Wi-Fi, and electrical noise of power supply. Table 10 is correlated with Table 11, as shown in Table 13. The relative errors in Table 13 are similar to Table 12 because the measured voltages of Table 11 are calculated by linear Equation (6). Another reason of higher relative errors is that the small value of linear Equation (6) results in the large difference, even if differences between small capacitances and linear Equation (6) are same as the differences between large capacitances and linear Equation (6).

B. CCPP SENSOR

The capacitances to pressures of CCPP sensor is illustrated in Table 14, and a linear equation (curve fitting) is calculated using MATLAB, which can be expressed as follows:

$$Capacitance(\text{pF}) = 0.0016 \times Pressure(\text{kPa}) + 3.6853. \quad (7)$$

As shown in Fig. 27(a), each cell of the CCPP sensor has differences between each other due to process variation; however, each cell nearly has the same trend on the measurement of pressure. Table 15 shows the relative errors of CCPP sensor according to linear Equation (7). The differences between each cell of CCPP sensor and linear Equation (7) are shown in Table 16 and Fig. 27(b).

Table 17 shows the relative errors according to the following fitting curve equation:

$$Capacitance(\text{pF}) = -4.2171 \times 10^{-7} \times Pressure^2(kPa^2) + 0.0027 \times \text{Pressure(kPa)} + 3.1656. \quad (8)$$

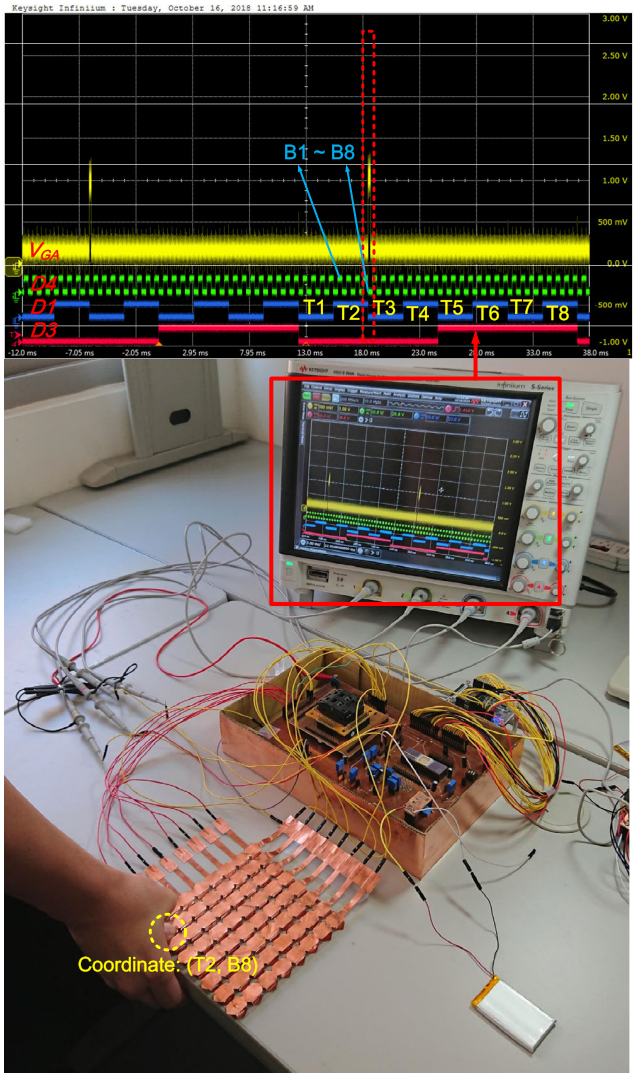

FIGURE 24. Pressing a cell on the proposed CCA to show the result on an oscilloscope.

Table 18 shows the differences between Table 14 and Equation (8). The display value on the display interface is converted by an equation. Thus, Equation (8) can be utilized to be a compensated transfer function to approximate the trend as Table 14. Fig. 28 shows the capacitances of CCPP sensor relative to Equation (8).

Fig. 29(a) shows a foot placed on the surface of the proposed CCPP sensor with the prototype detection system, and the measured result is revealed on a display interface depicted in Fig. 29(b).

C. 10-BIT FULLY DIFFERENTIAL SAR ADC

Fig. 30(a) demonstrates the measured output power spectrum of the proposed SAR ADC when a 113.2 Hz and 3.2 V_{pp} sinusoidal input is applied, and the sample rate is 5 kHz with a supply voltage of 3.3 V. Moreover, 32768 FFT points are computed. The measured signal-to-noise and distortion ratio and spurious-free dynamic range are 58.16 and 74.89 dB, respectively. Fig. 30(b) displays the measured differential

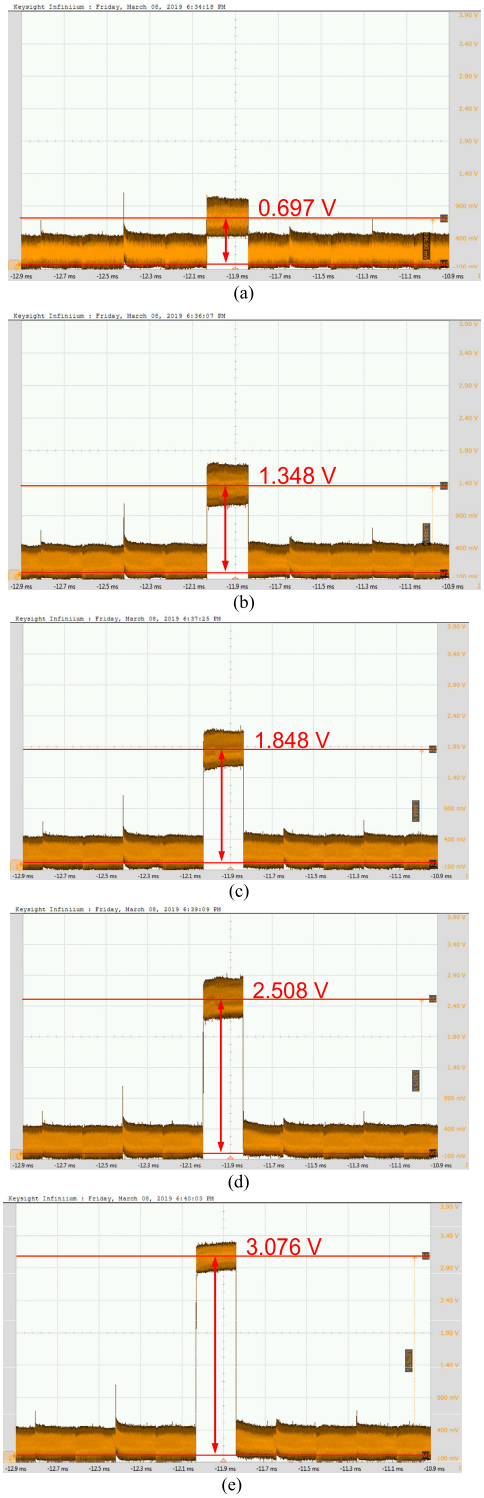

FIGURE 25. Using testing capacitors for calibration with capacitance of (a) 1.177 pF, (b) 2.246 pF, (c) 3.045 pF, (d) 3.923 pF, and (e) 5.405pF.

nonlinearity (DNL) and integral nonlinearity (INL), which are less than 1 LSB.

D. DISPLAY INTERFACE

Given the high stress of the proposed CCA, Fig. 31 shows a weight used to generate force on the CCA. The measurement

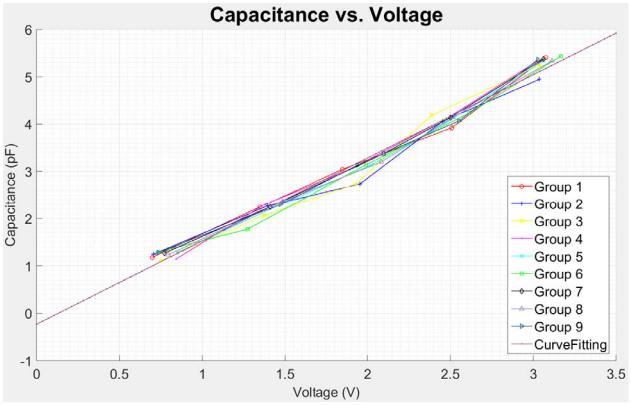

FIGURE 26. Comparison of nine groups with the linear equation (6).

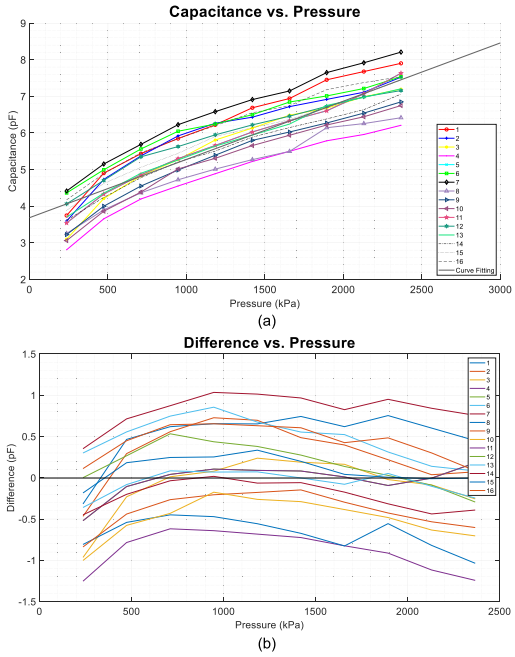

FIGURE 27. (a) Capacitances of CCPP sensor relative to pressures with linear Equation (7). (b) Differences between each cell of CCPP sensor and linear Equation (7).

of the CVC output is demonstrated on the oscilloscope screen, and the real-time variations of the CCA are shown on the GUI of a laptop via the FPGA. The color temperature map displays the bottom shape of the weight. The measurement result reveals the achievement of the proposed CCA and the detection system.

V. DISCUSSION

The capacitances of a group of commercial capacitors (1–5 pF) measured by an LCR meter are 1.109, 2.147, 3.035, 4.047, and 5.252 pF. The voltages via the CVC of the group are measured 10 times, as shown in Table 19. The linear equation of the group is calculated by MATLAB, as shown as follows:

$$Voltage = 0.5296 \times Capacitance - 0.0932. \quad (9)$$

TABLE 14. Capacitances relative to pressures of CCPP sensor.

Pressure (N)	40	80	120	160	200
Pressure (kPa)	237	473	710	947	1183
Position	Capacitance (pF)				
1	3.745	4.903	5.434	5.847	6.221
2	3.595	4.731	5.373	5.919	6.265
3	3.097	4.208	4.827	5.271	5.806
4	2.809	3.654	4.197	4.551	4.886
5	3.542	4.332	4.856	5.297	5.658
6	4.362	4.994	5.562	6.047	6.243
7	4.414	5.152	5.688	6.226	6.582
8	3.254	3.898	4.366	4.721	5.012
9	3.224	3.999	4.55	4.986	5.391
10	3.06	3.862	4.384	5.017	5.307
11	4.063	4.705	5.348	5.628	5.948
12	3.636	4.333	4.872	5.252	5.516
13	3.702	4.356	4.899	5.261	5.64
14	3.613	4.238	4.779	5.209	5.504
15	3.878	4.621	5.061	5.444	5.903
16	4.173	4.887	5.458	5.846	6.199
Pressure (N)	240	280	320	360	400
Pressure (kPa)	1420	1657	1893	2130	2367
Position	Capacitance (pF)				
1	6.688	6.941	7.452	7.677	7.902
2	6.431	6.719	6.917	7.112	7.524
3	6.134	6.485	6.677	6.988	7.196
4	5.221	5.498	5.786	5.958	6.209
5	6.027	6.332	6.605	7.071	7.632
6	6.499	6.845	7.011	7.214	7.535
7	6.912	7.147	7.649	7.917	8.208
8	5.272	5.496	6.143	6.256	6.416
9	5.798	6.026	6.272	6.542	6.849
10	5.656	5.937	6.217	6.442	6.748
11	6.22	6.459	6.727	6.986	7.158
12	5.987	6.162	6.32	6.747	6.896
13	5.943	6.243	6.751	6.972	7.206
14	5.886	6.148	6.383	6.637	7.061
15	6.144	6.363	6.705	7.064	7.448
16	6.551	6.747	7.182	7.376	7.537

The relative errors of the group according to linear Equation (9) is shown in Table 20, and the differences between the group and linear Equation (9) are shown in Table 21. The maximum positive relative error is 6.23%, and the maximum negative relative error is −14.41%. As shown in Fig. 32, the relation of capacitances and Equation (9) is calculated by MATLAB.

Tables 22 and 23 respectively show the relative errors and the differences of one group of commercial capacitors according to the following curve equation (cubic equation in one unknown):

$$Voltage = -0.0044 \cdot Capacitance^3 + 0.0132 \cdot Capacitance^2 + 0.5966 \cdot Capacitance - 0.2365. \quad (10)$$

Fig. 33 shows the calculation by MATLAB. The transfer function can utilize Equation (10); thus, repeatability will be

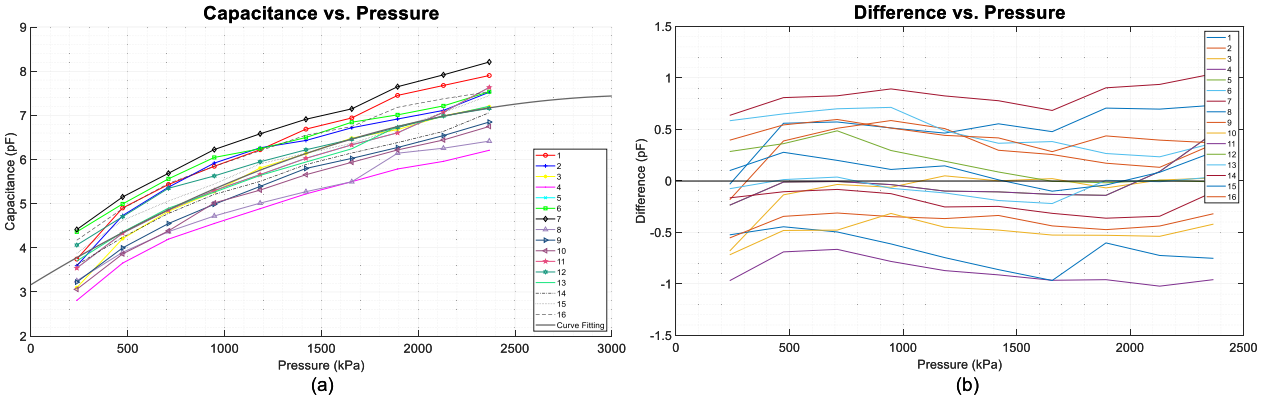

FIGURE 28. (a) Capacitances of CCPP sensor relative to pressures with the curve Equation (8). (b) Differences between each cell of CCPP sensor and the fitting curve Equation (8).

TABLE 15. Relative errors of CCPP sensor according to linear equation (7).

Pressure (N)	40	80	120	160	200
Pressure (kPa)	237	473	710	947	1183
Position	Relative Error (%)				
1	−7.8	10.46	12.85	12.62	11.71
2	−11.5	6.59	11.58	14	12.5
3	−23.76	−5.2	0.24	1.52	4.26
4	−30.85	−17.68	−12.84	−12.35	−12.26
5	−12.8	−2.4	0.84	2.02	1.6
6	7.39	12.51	15.51	16.47	12.11
7	8.67	16.07	18.12	19.91	18.2
8	−19.89	−12.18	−9.33	−9.07	−10
9	−20.63	−9.91	−5.51	−3.97	−3.19
10	−24.67	−12.99	−8.96	−3.37	−4.7
11	−12.8	−2.4	0.84	2.02	1.6
12	0.02	6	11.06	8.4	6.81
13	−8.86	−1.86	1.74	1.33	1.28
14	−11.05	−4.52	−0.75	0.33	−1.16
15	−4.53	4.11	5.1	4.85	6
16	2.73	10.1	13.35	12.6	11.32
Pressure (N)	240	280	320	360	400
Pressure (kPa)	1420	1657	1893	2130	2367
Position	Relative Error (%)				
1	12.49	9.79	11.24	8.5	6.04
2	8.17	6.28	3.26	0.52	0.97
3	3.17	2.58	−0.32	-1.24	-3.44
4	−12.18	−13.03	−13.63	-15.79	-16.68
5	1.37	0.16	−1.4	-0.06	2.41
6	9.31	8.27	4.66	1.96	1.11
7	16.26	13.05	14.19	11.89	10.14
8	−11.33	−13.07	−8.3	-11.58	-13.9
9	−2.48	−4.68	−6.37	-7.54	-8.09
10	−4.87	−6.09	−7.19	-8.95	-9.45
11	1.37	0.16	−1.4	-0.06	2.41
12	4.62	2.17	0.42	-1.26	-3.95
13	−0.04	−1.25	0.78	-1.46	-3.3
14	−1	−2.75	−4.71	-6.2	-5.25
15	3.34	0.65	0.09	-0.16	-0.05
16	10.19	6.72	7.21	4.25	1.14

TABLE 16. Differences of each cell of CCPP sensor according to linear equation (7).

Pressure (N)	40	80	120	160	200
Pressure (kPa)	237	473	710	947	1183
Position	Capacitance (pF)				
1	−0.317	0.4643	06187	0.655	0.6523
2	−0.467	0.2923	0.5577	0.727	0.6963
3	−0.965	−0.2307	0.0117	0.079	0.2373
4	−1.253	−0.7847	−0.6183	−0.641	−0.6827
5	−0.52	−0.1067	0.0407	0.105	0.0893
6	0.3	05553	0.7467	0.855	0.6743
7	0.352	0.7133	0.8727	1.034	1.0133
8	−0.808	−0.5407	−0.4493	−0.471	−0.5567
9	−0.838	−0.4397	−0.2653	−0.206	−0.1777
10	−1.002	−0.5767	−0.4313	−0.175	−0.2617
11	-0.52	−0.1067	0.0407	0.105	0.0893
12	0.001	0.2663	0.5327	0.436	0.3793
13	−0.36	−0.0827	0.0837	0.069	0.0713
14	−0.449	−0.2007	−0.0363	0.017	−0.0647
15	−0.184	0.1823	0.2457	0.252	0.3343
16	0.111	0.4483	0.6427	0.654	0.6303
Pressure (N)	240	280	320	360	400
Pressure (kPa)	1420	1657	1893	2130	2367
Position	Capacitance (pF)				
1	0.7426	0.6189	0.7533	0.6016	0.4499
2	0.4856	0.3969	0.2183	0.0366	0.0719
3	0.1886	0.1629	−0.0217	−0.0874	−0.2561
4	−0.7244	−0.8241	−0.9127	−1.1174	−1.2431
5	0.0816	0.0099	−0.0937	−0.0044	0.1799
6	0.5536	0.5229	0.3123	0.1386	0.0829
7	0.9666	0.8249	0.9503	0.8416	0.7559
8	−0.6734	−0.8261	−0.5557	−0.8194	−1.0361
9	−0.1474	−0.2961	−0.4267	−0.5334	−0.6031
10	−0.2894	−0.3851	−0.4817	−0.6334	−0.7041
11	0.0816	0.0099	−0.0937	−0.0044	0.1799
12	0.2746	0.1369	0.0283	−0.0894	−0.2941
13	−0.0024	−0.0791	0.0523	−0.1034	−0.2461
14	−0.0594	−0.1741	−0.3157	−0.4384	−0.3911
15	0.1986	0.0409	0.0063	−0.0114	−0.0041
16	0.6056	0.4249	0.4833	0.3006	0.0849

precise, which can be expressed as

$$\begin{aligned} Repeatability &= 100\% - (RE_{CF+} - RE_{CF-}) \\ &= 100\% - (4.48\% + 5.79\%) = 89.73\%, \end{aligned} \tag{11}$$

where RE_{CF+} and RE_{CF-} are the maximum positive and negative relative errors of commercial capacitors according to Equation (10), respectively.

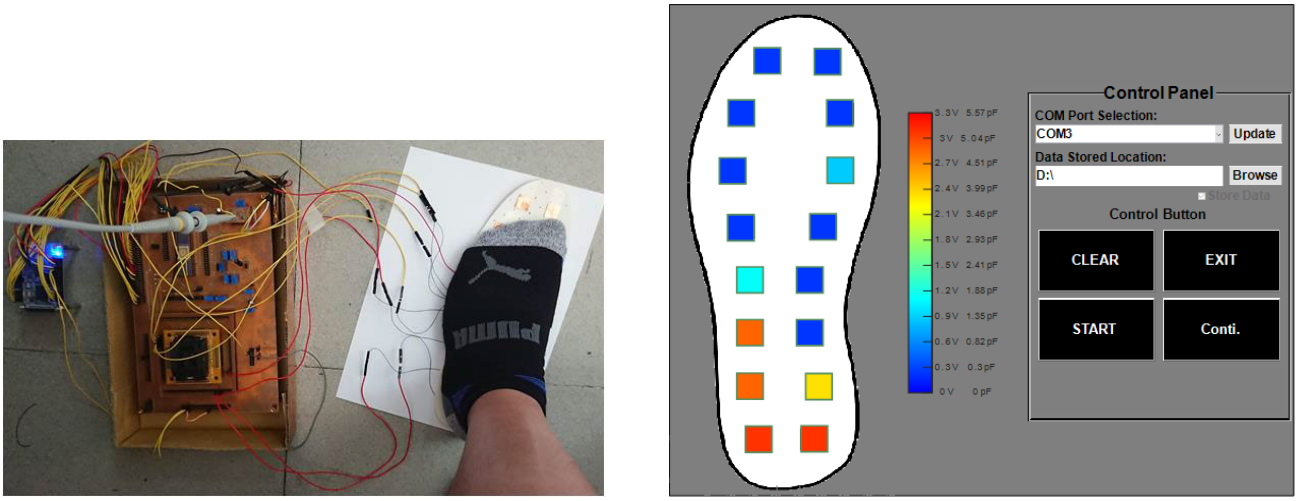

FIGURE 29. (a) Foot placed on the CCPP sensor with the detection system. (b) Display interface for CCPP sensor.

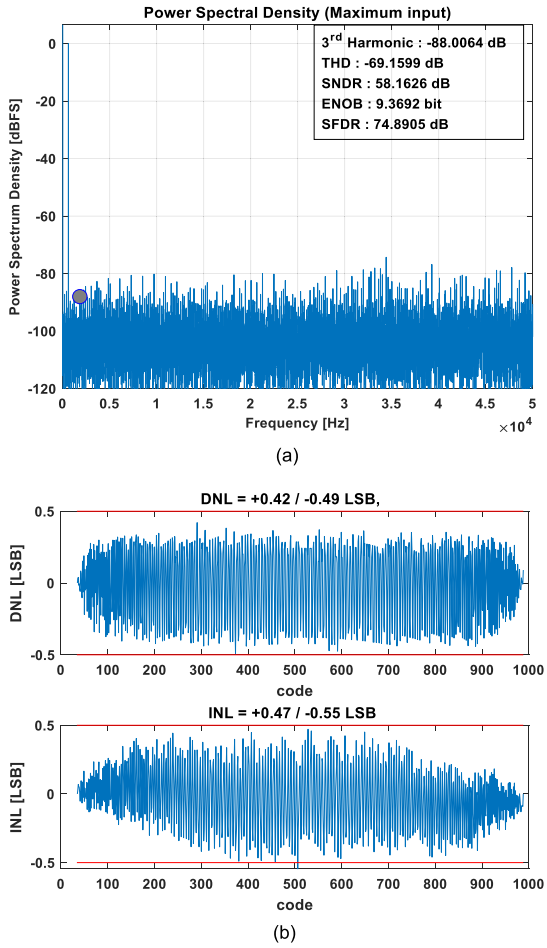

FIGURE 30. Measurements of the proposed SAR ADC. (a) Power. spectral density of the proposed SAR ADC. (b) DNL and INL of the proposed SAR ADC.

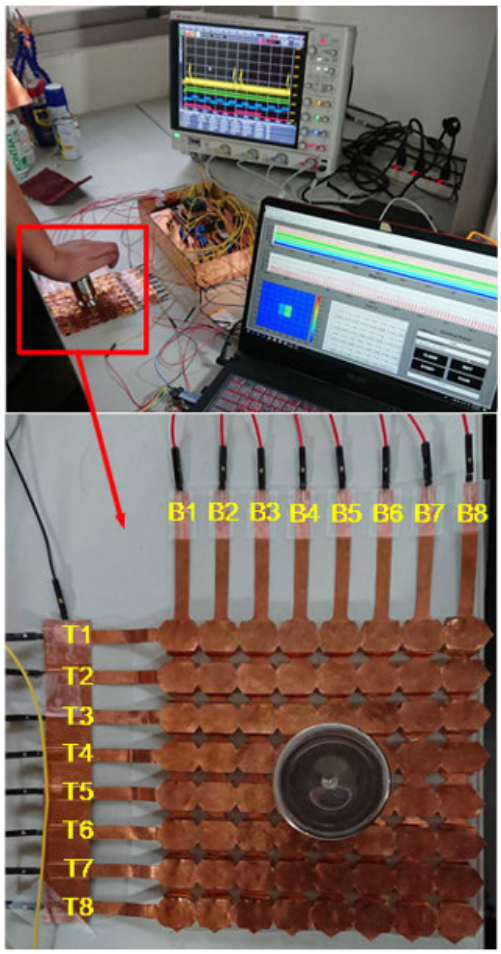

FIGURE 31. Weight used to generate force on the proposed CCA. The measured results are shown on the display interface.

To compare with similar approaches of plantar pressure monitoring, parameters as range of sensing capacitance, minimum sensing step, power consumption, accuracy, non-linearity, sensitivity, and repeatability are shown in Table 24.

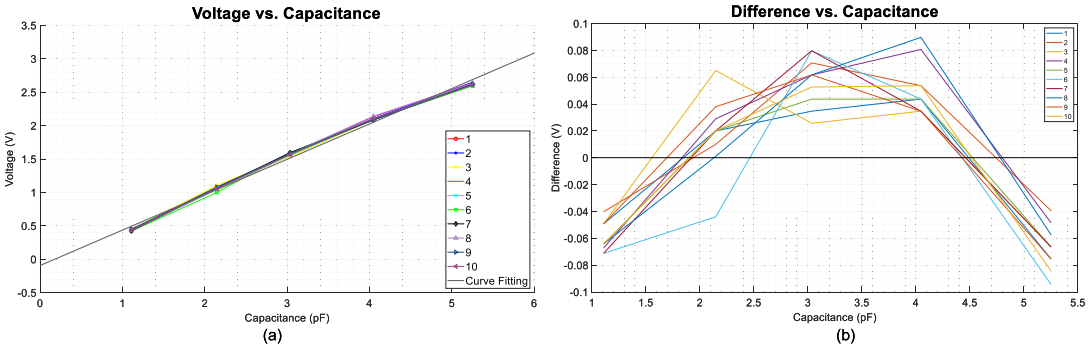

FIGURE 32. One group of commercial capacitors. (a) Measurement of the same group of commercial capacitors by 10 times with linear Equation.(9). (b) Differences between measurements and linear Equation (9).

TABLE 17. Relative errors of CCPP sensor according to curve equation (8).

Pressure (N)	40	80	120	160	200
Pressure (kPa)	237	473	710	947	1183
Position	Relative Error (%)				
1	−0.89	12.86	11.75	9.62	8.05
2	−4.86	8.9	10.5	10.97	8.81
3	−18.04	−3.13	−0.73	−1.18	0.84
4	−25.66	−15.89	−13.69	−14.68	−15.14
5	−6.26	−0.28	−0.14	−0.69	−1.73
6	15.44	14.96	14.38	13.37	8.43
7	16.82	18.6	16.97	16.73	14.32
8	−13.88	−10.27	−10.21	−11.49	−12.95
9	−14.68	−7.95	−6.43	−6.52	−6.37
10	−19.02	−11.1	−9.84	−5.94	−7.83
11	−6.26	−0.28	−0.14	−0.69	−1.73
12	7.53	8.31	9.98	5.52	3.31
13	−2.02	0.27	0.75	−1.36	−2.04
14	−4.38	−2.44	−1.72	−2.34	−4.41
15	2.63	6.37	4.08	2.07	2.52
16	10.44	12.5	12.24	9.6	7.66
Pressure (N)	240	280	320	360	400
Pressure (kPa)	1420	1657	1893	2130	2367
Position	Relative Error (%)				
1	9.03	7.38	10.47	9.97	10.23
2	4.84	3.95	2.54	1.88	4.96
3	0.006	0.33	−1.02	0.1	0.38
4	−14.89	−14.94	−14.23	−14.65	−13.39
5	−1.75	−2.04	−2.09	1.29	6.46
6	5.94	5.9	3.93	3.34	5.11
7	12.68	10.57	13.39	13.41	14.5
8	−14.06	−14.97	−8.94	−10.38	−10.5
9	−5.48	−6.77	−7.03	−6.29	−4.46
10	−7.8	−8.15	−7.84	−7.72	−5.87
11	−1.75	−2.04	−2.09	1.29	6.46
12	1.4	−0.74	−0.28	−0.72	−0.15
13	−3.12	−3.42	−0.74	−0.13	0.52
14	−4.05	−4.89	−5.38	−4.93	−1.5
15	0.16	−1.56	−0.61	1.19	3.9
16	6.79	4.38	6.46	5.66	5.14

To obtain the minimum sensing step, the procedure is described as

$$TC_{CV} = \frac{Capacitance}{Voltage} = \frac{1}{0.5296}\,\mathrm{pF/V} = 1.888\,\mathrm{pF/V}, \quad (12)$$

$$1.888\,\mathrm{pF/V} = \frac{C_{MINI}}{3.226\mathrm{mV}} \rightarrow C_{MINI} = 6.091\ \mathrm{fF}, \quad (13)$$

TABLE 18. Differences of each cell of CCPP sensor according to curve equation (8).

Pressure (N)	40	80	120	160	200
Pressure (kPa)	237	473	710	947	1183
Position	Capacitance (pF)				
1	−0.0335	0.5588	0.5714	0.5132	0.4633
2	−0.1835	0.3868	0.5104	0.5852	0.5073
3	−0.6815	−0.1362	−0.0356	−0.0628	0.0483
4	−0.9695	−0.6902	−0.6656	−0.7828	−0.8717
5	−0.2365	−0.0122	−0.0066	−0.0368	−0.0997
6	0.5835	0.6498	0.6994	0.7132	0.4853
7	0.6355	0.8078	0.8254	0.8922	0.8243
8	−0.5245	−0.4462	−0.4966	−0.6128	−0.7457
9	−0.5545	−0.3452	−0.3126	−0.3478	−0.3667
10	−0.7185	−0.4822	−0.4786	−0.3168	−0.4507
11	−0.2365	−0.0122	−0.0066	−0.0368	−0.0997
12	0.2845	0.3608	0.4854	0.2942	0.1903
13	−0.0765	0.0118	0.0364	−0.0728	−0.1177
14	−0.1655	−0.1062	−0.0836	−0.1248	−0.2537
15	0.0995	0.2768	0.1984	0.1102	0.1453
16	0.3945	0.5428	0.5954	0.5122	0.4413
Pressure (N)	240	280	320	360	400
Pressure (kPa)	1420	1657	1893	2130	2367
Position	Capacitance (pF)				
1	0.5536	0.4772	0.706	0.6961	0.7334
2	0.2966	0.2552	0.171	0.1311	0.3554
3	−0.0004	0.0212	−0.069	0.0071	0.0274
4	−0.9134	−0.9658	−0.96	−1.0229	−0.9596
5	−0.1074	−0.1318	−0.141	0.0901	0.4634
6	0.3646	0.3812	0.265	0.2331	0.3664
7	0.7776	0.6832	0.903	0.9361	1.0394
8	−0.8624	−0.9678	−0.603	−0.7249	−0.7526
9	−0.3364	−0.4378	−0.474	−0.4389	−0.3196
10	−0.4784	−0.5268	−0.529	−0.5389	−0.4206
11	−0.1074	−0.1318	−0.141	0.0901	0.4634
12	0.0856	−0.0048	−0.019	0.0051	−0.0106
13	−0.1914	−0.2208	0.005	−0.0089	0.0374
14	−0.2484	−0.3158	−0.363	−0.3439	−0.1076
15	0.0096	−0.1008	−0.041	0.0831	0.2794
16	0.4166	0.2832	0.436	0.3951	0.3684

$$\text{Minimum Sensing Step} = C_{MINI} \times [1 + (RE_+ - RE_-)]$$
$$= 6.091 \times (1 + 6.23\% + 14.41\%) = 7.348\mathrm{fF}. \quad (14)$$

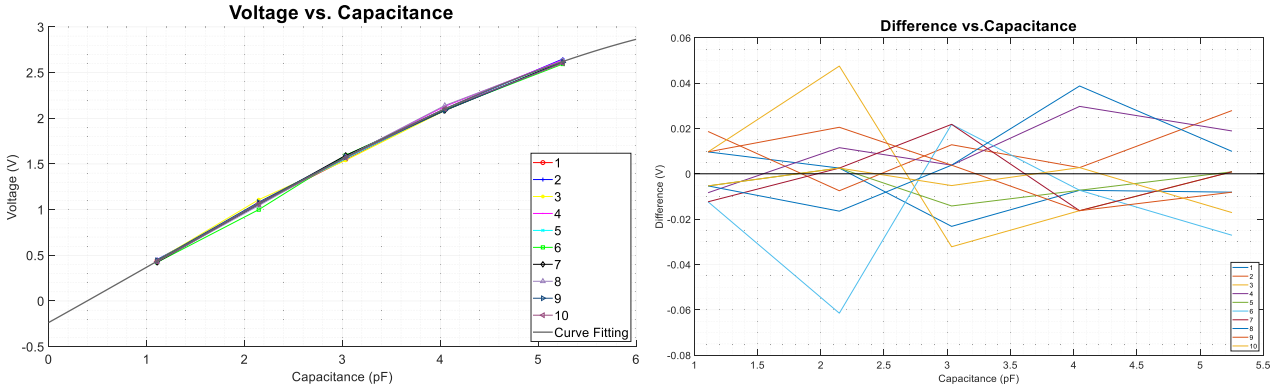

(a) (b)

FIGURE 33. One group of commercial capacitors. (a) Measurement of same group of commercial capacitors by 10 times with curve equation (10). (b) Differences between measurements and curve equation (10).

TABLE 19. Measured voltages of commercial capacitors.

Capacitance (pF)	Number of Times									
	1	2	3	4	5	6	7	8	9	10
1.109	0.445 V	0.454 V	0.445 V	0.427 V	0.43 V	0.423 V	0.423 V	0.43 V	0.445 V	0.43 V
2.147	1.064 V	1.054 V	1.109 V	1.073 V	1.064 V	1 V	1.064 V	1.045 V	1.082 V	1.064 V
3.035	1.549 V	1.585 V	1.54 V	1.576 V	1.558 V	1.594 V	1.594 V	1.576 V	1.576 V	1.567 V
4.047	2.094 V	2.104 V	2.085 V	2.131 V	2.094 V	2.094 V	2.085 V	2.14 V	2.085 V	2.104 V
5.252	2.613 V	2.649 V	2.622 V	2.64 V	2.622 V	2.594 V	2.622 V	2.631 V	2.613 V	2.604 V

TABLE 20. Relative errors of commercial capacitors according to linear equation (9).

Capacitance (pF)	Number of Times									
	1	2	3	4	5	6	7	8	9	10
1.109	−9.95%	−8.13%	−9.95%	−13.6%	−12.99%	−14.41%	−14.41%	−12.99%	−9.95%	−12.99%
2.147	1.92%	0.96%	6.23%	2.78%	1.92%	−4.21%	1.92%	0.1%	3.64%	1.92%
3.035	2.29%	4.67%	1.7%	4.08%	2.89%	5.26%	5.26%	4.08%	4.08%	3.48%
4.047	2.13%	2.62%	1.69%	3.94%	2.13%	2.13%	1.69%	4.38%	1.69%	2.62%
5.252	−2.81%	−1.47%	−2.47%	−1.8%	−2.47%	−3.51%	−2.47%	−2.14%	−2.81%	−3.14%

TABLE 21. Differences of commercial capacitors according to linear equation (9).

Capacitance (pF)	Number of Times									
	1	2	3	4	5	6	7	8	9	10
1.109	−49 mV	-−40 mV	−49 mV	−67 mV	−64 mV	−71 mV	−71 mV	−64 mV	−49 mV	−64 mV
2.147	20 mV	10 mV	65 mV	29 mV	20 mV	−44 mV	20 mV	1 mV	38 mV	20 mV
3.035	35 mV	71 mV	26 mV	62 mV	44 mV	80 mV	80 mV	62 mV	62 mV	53 mV
4.047	44 mV	54 mV	35 mV	81 mV	−44 mV	44 mV	35 mV	90 mV	35 mV	54 mV
5.252	−76 mV	−40 mV	−67 mV	−49 mV	−67 mV	−95 mV	−67 mV	−58 mV	−76 mV	−85 mV

where TC_{CV} is the transfer coefficient of Equation (8); **3.226 mV** is the 1 LSB of the 10-bit SAR ADC; C_{MINI} is the corresponding capacitance of **3.226 mV**; RE_+ and RE_- is the maximum positive and negative relative errors in Table 20, respectively. Thus, the minimum sensing step is 7.348 fF with RE_+ and RE_-.

Accuracy is calculated as follows:

$$\text{Accuracy} = 100\% - 14.41\% = 85.59\%. \tag{15}$$

where 14.41% is the maximum relative error in Table 20.

Another transfer coefficient (TC_{PC}) of pressure to capacitance can be obtained in Equation (16). Let the minimum sensing step be multiplied by TC_{PC}, and the sensitivity can be gained using Equation (17).

$$TC_{PC} = \frac{Pressure}{Capacitance} = \frac{1}{0.0016}\text{kPa}/\text{pF} = 625\text{kPa}/\text{pF} \tag{16}$$

$$\begin{aligned}\text{Sensitivity} &= \text{Minimum Sensing Step} \times TC_{PC} \\ &= 7.348 \times 10^{-3} \times 625 = 4.59\text{kPa}\end{aligned} \tag{17}$$

TABLE 22. Relative errors of commercial capacitors according to curve equation (10).

Capacitance (pF)	Number of Times									
	1	2	3	4	5	6	7	8	9	10
1.109	2.23%	4.3%	2.23%	−1.91%	-−1.22%	−2.83%	−2.83%	−1.22%	2.23%	−1.22%
2.147	0.24%	−0.7%	4.48%	1.09%	0.24%	−5.79%	0.24%	−1.55%	1.94%	0.24%
3.035	−1.47%	0.82%	−2.05%	0.24%	−0.9%	1.39%	1.39%	0.24%	0.24%	−0.33%
4.047	−0.34%	0.13%	−0.77%	1.42%	−0.34%	−0.34%	−0.77%	1.85%	−0.77%	0.13%
5.252	−0.31%	1.07%	0.04%	0.72%	0.04%	−1.03%	0.04%	0.38%	−0.31%	−0.65%

TABLE 23. Differences of commercial capacitors according to curve equation (10).

Capacitance (pF)	Number of Times									
	1	2	3	4	5	6	7	8	9	10
1.109	9.7 mV	18.7 mV	9.7 mV	−8.3 mV	−5.3 mV	−12.3 mV	−12.3 mV	−5.3 mV	9.7 mV	−5.3 mV
2.147	2.6 mV	−7.4 mV	47.6 mV	11.6 mV	2.6 mV	−61.4 mV	2.6 mV	−16.4 mV	20.6 mV	2.6 mV
3.035	−23.2 mV	12.8 mV	−32.2 mV	3.8 mV	−14.2 mV	21.8 mV	21.8 mV	3.8 mV	3.8 mV	−5.2 mV
4.047	−7.2 mV	2.8 mV	−16.2 mV	29.8 mV	-−7.2 mV	−7.2 mV	−16.2 mV	38.8 mV	−16.2 mV	2.8 mV
5.252	−8.1 mV	27.9 mV	0.927 mV	18.9 mV	0.927 mV	−27.1 mV	0.927 mV	9.9 mV	−8.1 mV	−17.1 mV

TABLE 24. Comparisons of similar approaches of plantar pressure monitoring.

Items	2012 [17]	2015 [18]	2018 [6]	2019 [19]	This work
Range of Sensing Capacitance	N/A	N/A	N/A	N/A	0 – 5.252 pF
Minimum Sensing Step	N/A	N/A	N/A	N/A	7.348fF
Power Consumption	N/A	3.7 V 140 mA	3.7 V 100 mA	N/A	3.3 V 80 mA (FPGA) 12 mA (Module)
Accuracy	N/A	N/A	N/A	N/A	85.59%
Sensitivity	N/A	5 kPa	N/A	2.5 kPa	4.6 kPa
Number of Sensors	4	32	8	13	16
Range of Pressure	0–1000 kPa	15–1000 kPa	0–6000 kPa	0–400 kPa	237–2367 kPa
Channels (Top + Bottom)	4 + 4	32 + 32	8 + 8	N/A	4 + 4

TABLE 25. Comparisons of similar capacitive acquisition modules for multipoint detection.

Items	2015 [20]	2017 [21]	2018 [22]	This Work
Type	Capacitive	Piezoresistive Capacitive	Capacitive	Capacitive
Complexity	$O(n)^2$	$O(n)^2$	$O(n)$	$O(n)$
Type of Array	$M \times N$	$M \times N$	$M + N$	$M + N$
Size of Array	4 × 6	4 × 12, 5 × 18	8 × 8	8 × 8
Total Detection Points	24	48, 90	64	64
I/O Ports for Sensor	Discrete	Discrete	Discrete	Integrated circuits
CVC/CDC	Discrete	Discrete	Discrete	Integrated circuits
Interface Connection	Wire	Wireless	Wire	Wire
Range of Sensing Capacitance	9.5–14 pF	0–16 pF	5–47 pF	0–5.252 pF
Minimum Sensing Step	1 fF	0.35 fF	0.3 pF	7.348 fF
Accuracy	N/A	84%	N/A	85.59%
Range of Pressure	100–180 kPa	25–150 kPa; 6–25 kPa	0–62.5 kPa	237–2367 kPa
Sensitivity	0.4–0.5 pF/N	0.77 pF/N or 1 pF/N	0.56 pF/N or 0.48 pF/N	0.01 pF/N
Repeatability	98.5%	88%; 79%	N/A	89.73%
Power Consumption	N/A	N/A	N/A	3.3 V 80 mA (FPGA) 12 mA (Module)

Table 24 shows the comparisons of similar approaches with the proposed method in this work; these approaches do not have considerable information. Moreover, other approaches all use the $M + N$ structure; thus, they need double wires for connection. Only the proposed method in this work use the $M \times N$ structure to reduce wires and hardware.

Table 25 presents a comparison, and the methods of the listed References [20]–[22] are similar to this approach with multipoint detection. The comparison reveals that the $M \times N$ array is used in References [20] and [21], and the quantity of DEMUXs is considerable (the input ports for sensors to receive input signals). In this work, the self-designed CVC has integrated several circuits. Therefore, the area including the acquisition module and idle pins can be reduced. The calculation of the linear equation of Table 14 is revised by Equations (18) and (19).

$$Capacitance(\text{pF}) = 0.0094 \times Pressure(\text{N}) + 3.6853 \quad (18)$$

$$\text{Sensitivity} = \frac{Capacitance}{Pressure} = 0.0094^{\text{pF}}/_{\text{N}} \quad (19)$$

VI. CONCLUSION

This study presents the detection system of the capacitance measurement for capacitive plantar pressure monitoring. The proposed detection system consists of a prototype acquisition module with a display interface and handmade cross-type capacitive sensors (i.e., cross-type capacitive array and cross-type capacitive plantar pressure sensor) for demonstrating the entire detection system. The supply voltage of the entire detection system is 3.3 V. The feature of the CVC is selectable for the detection points from 1 to 64, and it has the embedded functions of the CA and the self-separated input signal for capacitive sensors. The embedded function of CA can effectively reduce parasitic capacitances and influences of the temperature and relative humidity from the environment. The measured results shown on the display interfaces reveal the positions and amplitudes of the corresponding voltages. The conversion time for one capacitance is 0.4 ms, and the maximum conversion time for 64 capacitances is 25.6 ms. These findings indicate that real-time capacitive pressure sensors can be achieved.

REFERENCES

[1] S. Chakraborty, S. K. Bera, N. Mandal, and S. C. Bera, "Study on further modification of non-contact capacitance type-level transducer for a conducting liquid," *IEEE Sensors J.*, vol. 15, no. 11, pp. 6678–6688, Nov. 2015.
[2] S. Sinha, R. V. Kachhap, and N. Mandal, "Design and development of a capacitance-based wireless pressure transmitter," *IET Sci., Meas. Technol.*, vol. 12, no. 7, pp. 858–864, Oct. 2018.
[3] T. J. Salpavaara, J. A. Verho, J. O. Lekkala, and J. E. Halttunen, "Embedded capacitive sensor system for hip surgery rehabilitation: Online measurements and long-term stability," in *Proc. 30th Annu. Int. Conf. IEEE Eng. Med. Biol. Soc.*, Vancouver, BC, Canada, Aug. 2008, pp. 935–938.
[4] B. Saggin, D. Scaccabarozzi, and M. Tarabini, "Metrological performances of a plantar pressure measurement system," *IEEE Trans. Instrum. Meas.*, vol. 62, no. 4, pp. 766–776, Apr. 2013.
[5] X. Lin and B.-C. Seet, "Battery-free smart sock for abnormal relative plantar pressure monitoring," *IEEE Trans. Biomed. Circuits Syst.*, vol. 11, no. 2, pp. 464–473, Apr. 2017.
[6] P. Aqueveque, R. Osorio, F. Pastene, F. Saavedra, and E. Pino, "Capacitive sensors array for plantar pressure measurement insole fabricated with flexible PCB," in *Proc. 40th Annu. Int. Conf. IEEE Eng. Med. Biol. Soc. (EMBC)*, Honolulu, HI, USA, Jul. 2018, pp. 4393–4396.
[7] N. Hegde, M. Bries, T. Swibas, E. Melanson, and E. Sazonov, "Automatic recognition of activities of daily living utilizing insole-based and wrist-worn wearable sensors," *IEEE J. Biomed. Health Informat.*, vol. 22, no. 4, pp. 979–988, Jul. 2018.
[8] F. Lin, A. Wang, L. Cavuoto, and W. Xu, "Toward unobtrusive patient handling activity recognition for injury reduction among at-risk caregivers," *IEEE J. Biomed. Health Informat.*, vol. 21, no. 3, pp. 682–695, May 2017.
[9] L. Zhou and S. Chakrabartty, "Linearization of CMOS hot-electron injectors for self-powered monitoring of biomechanical strain variations," *IEEE Trans. Biomed. Circuits Syst.*, vol. 11, no. 2, pp. 446–454, Apr. 2017.
[10] F. Lin, A. Wang, Y. Zhuang, M. R. Tomita, and W. Xu, "Smart insole: A wearable sensor device for unobtrusive gait monitoring in daily life," *IEEE Trans Ind. Informat.*, vol. 12, no. 6, pp. 2281–2291, Dec. 2016.
[11] D. Chen, Y. Cai, and M.-C. Huang, "Customizable pressure sensor array: Design and evaluation," *IEEE Sensors J.*, vol. 18, no. 15, pp. 6337–6344, Aug. 2018.
[12] N. Lea, "Notes on the stability of LC oscillators," *J. Inst. Elect. Eng. III, Radio Commun. Eng.*, vol. 92, no. 20, pp. 261–274, Dec. 1945.
[13] Engineering ToolBox. (2004). *Water—Saturation Pressure*. Accessed: Oct. 14, 2019. [online] Available at: https://www.engineeringtoolbox.com/water-vapor-saturation-pressure-d_599.html
[14] B. K. Ahuja, "An improved frequency compensation technique for CMOS operational amplifiers," *IEEE J. Solid-State Circuits*, vol. 18, no. 6, pp. 629–633, Dec. 1983.
[15] D. Aksin, M. Al-Shyoukh, and F. Maloberti, "Switch bootstrapping for precise sampling beyond supply voltage," *IEEE J. Solid-State Circuits*, vol. 41, no. 8, pp. 1938–1943, Aug. 2006.
[16] C.-C. Liu, S.-J. Chang, G.-Y. Huang, and Y.-Z. Lin, "A 10-bit 50-MS/s SAR ADC with a monotonic capacitor switching procedure," *IEEE J. Solid-State Circuits*, vol. 45, no. 4, pp. 731–740, Apr. 2010.
[17] O. Mazumder, A. S. Kundu, and S. Bhaumik, "Development of wireless insole foot pressure data acquisition device," in *Proc. Int. Conf. Commun., Devices Intell. Syst. (CODIS)*, Kolkata, India, Dec. 2012, pp. 302–305.
[18] Y. S. A. Mustufa, J. Barton, B. O'Flynn, R. Davies, P. McCullagh, and H. Zheng, "Design of a smart insole for ambulatory assessment of gait," in *Proc. IEEE 12th Int. Conf. Wearable Implant. Body Sensor Netw. (BSN)*, Cambridge, MA, USA, Jun. 2015, pp. 9–12.
[19] T. P. Kakarla, K. A. Varma, P. S. P., J. Joseph, and M. Sivaprakasam, "Accuracy enhancement of total force by capacitive insoles," in *Proc. IEEE Int. Symp. Med. Meas. Appl. (MeMeA)*, Istanbul, Turkey, Jun. 2019, pp. 26–28.
[20] S. Cruz, D. Dias, J. C. Viana, and L. A. Rocha, "Inkjet printed pressure sensing platform for postural imbalance monitoring," *IEEE Trans. Instrum. Meas.*, vol. 64, no. 10, pp. 2813–2820, Oct. 2015.
[21] A. S. Naidu, R. V. Patel, and M. D. Naish, "Low-cost disposable tactile sensors for palpation in minimally invasive surgery," *IEEE/ASME Trans. Mechatronics*, vol. 22, no. 1, pp. 127–137, Feb. 2017.
[22] N. Xue, C. Liu, J. Sun, T. Li, C. Chi, H.-I. Hee, and Y.-S. Wang, "Miniature force sensing system for monitoring of optimal cricoid pressure for airway protection," *IEEE Sensors J.*, vol. 18, no. 10, pp. 4303–4310, May 2018.

TZUNG-MIN TSAI (Student Member, IEEE) was born in Changhua, Taiwan, in 1988. He received the B.S. degree from National Kaohsiung Normal University, in 2010, and the M.S. degree from National Chi Nan University, in 2012, Taiwan. He is currently pursuing the Ph.D. degree with the Department of Electrical Engineering, National Cheng Kung University, Taiwan.

His research interest includes system-level sensing design.

SHUENN-YUH LEE (Senior Member, IEEE) was born in Taichung, Taiwan, in 1966. He received the B.S. degree from the National Taiwan Ocean University, Keelung, Taiwan, in 1988, and the M.S. and Ph.D. degrees from the National Cheng Kung University, Tainan, Taiwan, in 1994 and 1999, respectively.

He is currently a Professor with the Department of Electrical Engineering, National Cheng Kung University. His present research activities involve the design of analog and mixed-signal integrated circuits, biomedical circuits and systems, low-power and low-voltage analog circuits, and RF front-end integrated circuits for wireless communications.

Dr. Lee is also a member of Circuits and Systems (CAS) Society, Solid-State Circuits Society, and Medicine and Biology Society of IEEE. He is also a member of IEICE. He served as the Technical Program Chair (TPC) for the 2014/2015 International Symposium on Bioelectronics and Bioinformatics (ISBB), and the 2015 Taiwan and Japan Conference on Circuits and Systems (TJCAS). From 2013 to 2016, he served as the Chairman for IEEE Solid-State Circuits Society Tainan Chapter. From 2016 to 2017, he served as the Vice Chairman for the IEEE Tainan Section. Since 2016, he has been serving as the Associate Editor for the IEEE TRANSACTION ON BIOMEDICAL CIRCUITS AND SYSTEMS.

SOON-JYH CHANG (Member, IEEE) was born in Tainan, Taiwan, in 1969. He received the B.S. degree in electrical engineering from National Central University, Taiwan, and the M.S. and Ph.D. degrees in electronic engineering from National Chiao Tung University, Taiwan, in 1991, 1996, and 2002, respectively. He joined the Department of Electrical Engineering, National Cheng Kung University, Taiwan, in 2003, where he has been a Professor, since 2011. His research interests include design, testing, and design automation for analog and mixed-signal circuits. He was one of the recipients of the Greatest Achievement Award from National Science Council, Taiwan, in 2007 and 2013. In 2010, he received the Best Paper Award from the Institute of Electronics, Information and Communication Engineers, and the Best Gold Member Award from the IEEE Tainan Section. Also, he was a recipient of the Gold and Diamond Prizes of the Macronix Golden Silicon Award, in 2010, 2015, and 2016. He served as the Chair for the IEEE SSCS Tainan Chapter, from 2009 to 2012, the Technical Program Co-Chair for the 2010 IEEE International Symposium on Next-Generation Electronics, and a Committee Member for the IEEE VLSI Design Automation and Test and the IEEE Asian Solid-State Circuits Conference in the past few years.